Aerosol and Cloud Experiments in the Eastern North Atlantic (ACE-ENA)

Jian Wang,[a,b] Rob Wood,[c] Michael P. Jensen,[b] J. Christine Chiu,[d] Yangang Liu,[b] Katia Lamer,[b] Neel Desai,[b] Scott E. Giangrande,[b] Daniel A. Knopf,[e] Pavlos Kollias,[e,b] Alexander Laskin,[f,g] Xiaohong Liu,[h] Chunsong Lu,[i] David Mechem,[j] Fan Mei,[k] Mariusz Starzec,[l] Jason Tomlinson,[k] Yang Wang,[a,m] Seong Soo Yum,[n] Guangjie Zheng,[a] Allison C. Aiken,[o] Eduardo B. Azevedo,[p] Yann Blanchard,[q] Swarup China,[k] Xiquan Dong,[r] Francesca Gallo,[o] Sinan Gao,[i] Virendra P. Ghate,[s] Susanne Glienke,[k] Lexie Goldberger,[k] Joseph C. Hardin,[k] Chongai Kuang,[b] Edward P. Luke,[b] Alyssa A. Matthews,[k] Mark A. Miller,[t] Ryan Moffet,[u] Mikhail Pekour,[k] Beat Schmid,[k] Arthur J. Sedlacek,[b] Raymond A. Shaw,[v] John E. Shilling,[k] Amy Sullivan,[w] Kaitlyn Suski,[k*] Daniel P. Veghte,[k#] Rodney Weber,[x] Matt Wyant,[c] Jaemin Yeom,[n,v] Maria Zawadowicz,[k,&] and Zhibo Zhang[y]

[a] *Center for Aerosol Science and Engineering, Department of Energy, Environmental and Chemical Engineering, Washington University in St. Louis, St. Louis, Missouri, USA*

[b] *Environmental and Climate Science Department, Brookhaven National Laboratory, Upton, New York, USA*

[c] *Department of Atmospheric Science, University of Washington, Seattle, Washington, USA*

[d] *Department of Atmospheric Science, Colorado State University, Fort Collins, CO, USA*

[e] *School of Marine and Atmospheric Sciences, Stony Brook University, Stony Brook, NY, USA.*

[f] *Department of Chemistry, Purdue University, West Lafayette, Indiana, USA*

[g] *Department of Earth, Atmospheric, and Planetary Sciences, Purdue University, West Lafayette, Indiana, USA*

[h] *Department of Atmospheric Sciences, Texas A&M University, College Station, Texas, USA*

[i] *Collaborative Innovation Center on Forecast and Evaluation of Meteorological Disasters, Key Laboratory for Aerosol-Cloud-Precipitation of China Meteorological Administration, Nanjing University of Information Science & Technology, Nanjing, China*

[j] *Department of Geography and Atmospheric Science, University of Kansas, Lawrence, Kansas, USA*

[k] *Pacific Northwest National Laboratory, Richland, Washington, USA*

[l] *Department of Atmospheric Sciences, University of North Dakota, Grand Forks, North Dakota, USA*

Early Online Release: This preliminary version has been accepted for publication in *Bulletin of the American Meteorological Society*, may be fully cited, and has been assigned DOI 10.1175/BAMS-D-19-0220.1. The final typeset copyedited article will replace the EOR at the above DOI when it is published.

[m] *Department of Civil, Architectural and Environmental Engineering, Missouri University of Science and Technology, Rolla, Missouri, USA*

[n] *Department of Atmosphere Science, Yonsei university, Seoul, Korea*

[o] *Earth and Environmental Sciences Division, Los Alamos National Laboratory, Los Alamos, NM, USA*

[p] *Centre of Climate, Meteorology and Global Change (CMMG), University of Azores, Angra do Heroísmo, Portugal*

[q] *ESCER Centre, Department of Earth and Atmospheric Sciences, University of Quebec at Montreal, Montreal, Quebec, Canada*

[r] *Department of Hydrology and Atmospheric Sciences, University of Arizona, Tucson, AZ, USA*

[s] *Argonne National Laboratory, Argonne, IL, USA*

[t] *Department of Environmental Sciences, Rutgers University, New Brunswick, New Jersey, USA*

[u] *Sonoma Technology Inc., Petaluma, CA, USA*

[v] *Atmospheric Sciences Program and Department of Physics, Michigan Technological University, Houghton, Michigan, USA*

[w] *Department of Atmospheric Science, Colorado State University, Fort Collins, Colorado, USA*

[x] *School of Earth and Atmospheric Sciences, Georgia Institute of Technology, Atlanta, GA, USA*

[y] *Physics Department, University of Maryland Baltimore County (UMBC), Baltimore, MD, USA*

* *Current affiliation: JUUL Labs, San Francisco, CA, USA*

[#] *Current affiliation: Ohio State University, Columbus, OH, USA*

[&] *Current affiliation: Environmental and Climate Science Department, Brookhaven National Laboratory, Upton, New York, USA*

Corresponding author: Jian Wang, jian@wustl.edu

Accepted for publication in *Bulletin of the American Meteorological Society*. DOI 10.1175/BAMS-D-19-0220.1.

ABSTRACT

With their extensive coverage, marine low clouds greatly impact global climate. Presently, marine low clouds are poorly represented in global climate models, and the response of marine low clouds to changes in atmospheric greenhouse gases and aerosols remains the major source of uncertainty in climate simulations. The Eastern North Atlantic (ENA) is a region of persistent but diverse subtropical marine boundary layer clouds, whose albedo and precipitation are highly susceptible to perturbations in aerosol properties. In addition, the ENA is periodically impacted by continental aerosols, making it an excellent location to study the cloud condensation nuclei (CCN) budget in a remote marine region periodically perturbed by anthropogenic emissions, and to investigate the impacts of long-range transport of aerosols on remote marine clouds. The Aerosol and Cloud Experiments in Eastern North Atlantic (ACE-ENA) campaign was motivated by the need of comprehensive in-situ measurements for improving the understanding of marine boundary layer CCN budget, cloud and drizzle microphysics, and the impact of aerosol on marine low cloud and precipitation. The airborne deployments took place from June 21 to July 20, 2017 and January 15 to February 18, 2018 in the Azores. The flights were designed to maximize the synergy between in-situ airborne measurements and ongoing long-term observations at a ground site. Here we present measurements, observation strategy, meteorological conditions during the campaign, and preliminary findings. Finally, we discuss future analyses and modeling studies that improve the understanding and representation of marine boundary layer aerosols, clouds, precipitation, and the interactions among them.

Accepted for publication in *Bulletin of the American Meteorological Society.* DOI 10.1175/BAMS-D-19-0220.1.

CAPSULE (BAMS ONLY)

Comprehensive in-situ and remote sensing measurements during the ACE-ENA campaign allow for improved understanding of aerosols, clouds, precipitation, and interactions among them in remote marine environment.

Accepted for publication in *Bulletin of the American Meteorological Society.* DOI 10.1175/BAMS-D-19-0220.1.

There are large uncertainties in the magnitude of the global aerosol radiative forcing (Lohmann and Feichter 2005; IPCC 2013; Bellouin et al. 2020). Major contributions to this uncertainty derive from poor understanding of cloud and precipitation processes (Gettelman et al. 2013), the cloud and precipitation responses to aerosol changes (Rosenfeld et al. 2014b; Rosenfeld et al. 2014a), and the natural aerosol state that is being perturbed by anthropogenic emissions (Carslaw et al. 2013). Remote marine low cloud systems are particularly susceptible to perturbations in aerosol properties associated with anthropogenic emissions because of relatively low cloud optical thickness and background aerosol concentrations (Twomey 1977; Carslaw et al. 2013; Wang et al. 2019b). Indeed, studies found that a large fraction of the global aerosol indirect forcing can be attributed to the changes in marine low clouds (Kooperman et al. 2013), despite their relatively long distance from most anthropogenic sources. The responses of low cloud systems to changes in atmospheric aerosols are among the major sources of uncertainty that limit our ability to predict future climate (Bony and Dufresne 2005; Lohmann and Feichter 2005; Wang et al. 2019b). Precipitation processes that impact the natural cloud and aerosol states are also important for setting cloud feedbacks to greenhouse gases (Bodas-Salcedo et al. 2019), highlighting the importance of aerosol-cloud interactions not only for aerosol radiative forcing but also for the cloud feedbacks. Next, we overview the current understanding and knowledge gaps in four interconnected topical areas on aerosol, cloud, and precipitation that are critical to quantifying the aerosol indirect forcing of marine low clouds and the feedbacks to greenhouse gases.

Mechanisms controlling the aerosol population in the marine boundary layer

Vertically transported aerosol from free troposphere represents a major source of boundary layer particles in remote environments (Raes 1995; Wang et al. 2016b). Over the mid-latitude

Accepted for publication in *Bulletin of the American Meteorological Society.* DOI 10.1175/BAMS-D-19-0220.1.

oceans, boundary layer aerosol is continually being modified by entrained free troposphere air with a time scale ranging from hours to several days. The sources of the free troposphere aerosol include long-range transport of continental emissions (e.g., Zheng et al. 2020c), and new particle formation in the outflow regions of distant deep convection (e.g., Clarke et al. 1998). Some of the free troposphere particles entrained into the marine boundary layer (MBL) readily serve as CCN (Wood et al. 2012), whereas others require condensational growth to reach sufficient sizes (Russell et al. 1998; Quinn and Bates 2011; Frossard et al. 2014; Zheng et al. 2018; Zheng et al. 2020a). While it has long been recognized that sulfate produced from dimethyl sulfide (DMS) oxidation is a major species for particle condensational growth in the remote marine environment (e.g., Charlson et al. 1987), recent studies suggest that secondary organics may also contribute to the particle condensational growth in the MBL (Quinn and Bates 2011; Willis et al. 2017; Brüggemann et al. 2018). At present, the contribution of secondary organics to the particle growth in the MBL and the seasonal variation of this contribution are not clear. Nucleation and formation of new particles in the MBL have mostly been observed when the surface area of pre-existing aerosol was low under conditions of low wind and strong precipitation (Petters et al. 2006; Wood et al. 2011). However, the impact of new particle formation inside the MBL on CCN population and marine low clouds remains poorly understood. Sea spray aerosol (SSA) can also contribute substantially to the MBL CCN population (O'Dowd et al. 2004; Prather et al. 2013; Quinn et al. 2015). In the MBL, the main loss mechanism for CCN is coalescence scavenging, namely the process of drizzle drops accreting cloud droplets (Feingold et al. 1996; Wood et al. 2012). The loss by coalescence scavenging is a strong function of precipitation rate, which is influenced by aerosol itself and likely depends on the mesoscale structure of low clouds as discussed below. .

Accepted for publication in *Bulletin of the American Meteorological Society.* DOI 10.1175/BAMS-D-19-0220.1.

Effects of Aerosol on Clouds and Precipitation

Twomey (1977) first suggested that variations in aerosol concentration change cloud droplet number concentration (N_d), a phenomenon that was later confirmed using ground-based and airborne measurements (e.g., Feingold et al. 2003; Painemal and Zuidema 2013). A change in N_d also modifies the cloud droplet size and therefore the efficiency of precipitation formation (Albrecht 1989), which can alter the macrophysical properties of low clouds. In the last decade, numerous field observations and modeling studies have confirmed that drizzle is strongly susceptible to the variations in N_d and CCN concentration (Hudson and Yum 2001; Feingold and Siebert 2009; Sorooshian et al. 2010; Terai et al. 2012; Mann et al. 2014), but the cloud responses to drizzle suppression are complex and challenging to observe. Suppression of drizzle by anthropogenic aerosol allows clouds to retain more condensate, potentially leading to a further increase in cloud albedo (Albrecht 1989). However, drizzle suppression also drives stronger turbulence and entrainment of free troposphere air (Ackerman et al. 2004; Wood 2007), possibly resulting in cloud thinning and subsequent decrease in albedo. Aircraft observations of ship tracks (Chen et al. 2012) confirm earlier satellite studies (e.g., Coakley and Walsh 2002) in showing that cloud condensate responses to CCN increases can be either positive or negative, depending upon several aspects of the cloud state being perturbed, including cloud base height (Wood 2007; Chen et al. 2011) and the dryness of the free troposphere (Ackerman et al. 2004; Christensen and Stephens 2011). It is likely that the susceptibility of precipitation to aerosol concentration also depends on cloud type (e.g., shallower stratocumulus vs. deeper convective clouds) and state (e.g., Stevens and Feingold 2009). However, studies disagree about the magnitude of the susceptibility (L'Ecuyer et al. 2009; Wood et al. 2009; Terai et al. 2015) and how the susceptibility varies with the cloud type

Accepted for publication in *Bulletin of the American Meteorological Society.* DOI 10.1175/BAMS-D-19-0220.1.

(Sorooshian et al. 2010; Mechem et al. 2012; Terai et al. 2012; Terai et al. 2015), leaving a significant knowledge gap that has major impact on the magnitude of aerosol indirect effects.

Cloud Microphysical and Macrophysical Structures, and Entrainment Mixing

As follows from the discussion above, improved understanding of the microphysics and macrophysical structures of precipitating low clouds under a broad range of meteorological and cloudiness conditions is needed to quantify the sensitivity of the low cloud systems to aerosols and meteorology. The entrainment of free troposphere air into the cloud topped MBL has important consequences for the thermodynamic structure as well as cloud macro- and microphysical properties. Entrainment of warm, dry free troposphere air into the cloudy MBL results in evaporation of cloud droplets and subsequent deviations from adiabatic liquid water profiles (Nicholls and Leighton 1986; Gerber 1996). These effects strongly influence the macrophysical structure of MBL clouds. The magnitude of cloud-top entrainment is driven by the strength of vertical gradients in buoyancy and horizontal winds in the entrainment interfacial layer (Wang and Albrecht 1994; Gerber et al. 2005; Albrecht et al. 2016). However, how the entrainment rate of free troposphere air into cloud topped MBL relates to the turbulence remains one of the main unresolved questions of MBL dynamics. Boundary layer turbulence is strongly modulated by cloud processes, so interactions between clouds, turbulence and entrainment are of major importance for cloud-climate feedback (Bretherton 2015). Equally important is the subsequent turbulent mixing process and its effects on cloud microphysics (Lehmann et al. 2009; Lu et al. 2011; Yum et al. 2015). Following Warner (1973) and Baker et al. (1980), entrainment-mixing processes can be homogeneous or inhomogeneous based on the ratio of turbulent mixing time and droplet evaporation time defined as the Damkoehler number (D_a). In the homogeneous mixing scenario, turbulent mixing is much faster than droplet evaporation and all droplets evaporate simultaneously; in the extreme

Accepted for publication in *Bulletin of the American Meteorological Society.* DOI 10.1175/BAMS-D-19-0220.1.

inhomogeneous mixing scenario, turbulent mixing is slow compared to droplet evaporation and some droplets evaporate completely while others do not evaporate at all. The intimate connections among the microphysical, dynamical, and thermodynamic properties associated with different entrainment mixing processes remains the focus of active investigation (Lu et al. 2013b; Lu et al. 2013a; Yeom et al. 2017; Pinsky and Khain 2018; Hoffmann and Feingold 2019). The dependence of the entrainment mixing process on spatial scale and altitude also needs to be further elucidated (Burnet and Brenguier 2007; Wang et al. 2009; Lu et al. 2014; Yum et al. 2015; Kumar et al. 2018).

Evaluating and improving the current retrievals of MBL cloud and drizzle properties from ground-based remote sensing

Drizzle plays a crucial role in determining the lifecycle of maritime warm clouds. Currently, many weather and climate models struggle to produce drizzle with the right amount and frequency (Stephens et al. 2010; Wyant et al. 2015). This demonstrates the need for concurrent estimates of cloud and drizzle microphysical properties that can help to improve our process-level understanding of drizzle formation. However, characterizing properties of drizzling clouds from remote sensing observations is challenging. The challenge arises from the difficulty in separating cloud and drizzle, as cloud signals are obscured by coexisting drizzle drops that dominate radar returns. To overcome this obstacle, some methods use radar Doppler spectra to separate signals from cloud and embryonic precipitation particles (Luke and Kollias 2013; Nguyen and Chandrasekar 2014; Joshil et al. 2020), which are useful for identifying drizzle initiation and understanding the associated trigger conditions. Quantitative drizzle microphysical properties in sub-cloud layers can be obtained by combining observations from radar and lidar (O'Connor et al. 2005; Wu et al. 2015) or multi-wavelength lidars (Westbrook et al. 2010; Lolli et al. 2013). In contrast, for retrieving in-cloud drizzle properties, the methods

Accepted for publication in *Bulletin of the American Meteorological Society.* DOI 10.1175/BAMS-D-19-0220.1.

typically require additional observational constraints from shortwave radiometer (Fielding et al. 2015) or microwave radiometer (Rusli et al. 2017; Cadeddu et al. 2020; Wu et al. 2020). All these methods provide invaluable cloud and drizzle properties, but their retreival quality has not been evaluated against in-situ measurements.

The Aerosol and Cloud Experiments in the Eastern North Atlantic (ACE-ENA) campaign was motivated by the need of comprehensive in-situ measurements for addressing the above knowledge gaps in aerosol and cloud processes, and validating and improving retrieval algorithms of surface-based remote sensing (Wang et al. 2016a). The ACE-ENA was conducted in the Azores, taking advantage of ongoing long-term ground-based measurements. The ACE-ENA campaign provided simultaneous in-situ characterizations of meteorological parameters, trace gases, aerosol, cloud, and drizzle fields under a variety of representative meteorological and cloud conditions, which are critical to understanding the key processes that drive the properties and interactions between aerosols, clouds, and precipitation.

Measurements and observation strategy

In October 2013, an atmospheric observatory (i.e., ENA site) was established on Graciosa Island in the Azores, Portugal (39° 5' 30" N, 28° 1' 32" W, 30.48 m above mean sea level) by the U.S. Department of Energy (DOE) Atmospheric Radiation Measurement (ARM) Climate Research Facility (Mather and Voyles 2013). The ENA site provides continuous measurements of atmospheric state, aerosols, clouds, and precipitation using a large array of state-of-the-art instruments/sensors (Table S1). The site straddles the boundary between the subtropics and mid-latitudes in the ENA, and experiences a great diversity of meteorological and cloud conditions (Remillard and Tselioudis 2015; Mechem et al. 2018; Giangrande et al. 2019). In

Accepted for publication in *Bulletin of the American Meteorological Society.* DOI 10.1175/BAMS-D-19-0220.1.

addition, the ENA site is often downwind of the North American continent and is periodically impacted by continental anthropogenic aerosols (Wood et al. 2015). Therefore, the site is an excellent location to study the CCN budget in a remote marine region periodically perturbed by anthropogenic emissions, and to investigate the impacts of long-range transport of aerosols on remote marine clouds. The ACE-ENA campaign was designed to take advantage of the ideal location and the long-term measurements at the ENA site. During the ACE-ENA campaign, the Gulfstream-1 (G-1) research aircraft of the ARM Aerial Facility (Schmid et al. 2014) was deployed in two intensive operational periods (IOPs) in summer of 2017 and in winter of 2018, respectively. Deployments during both seasons allow for examination of key aerosol and cloud processes under a variety of representative meteorological and cloud conditions. A total of 39 flights (20 during the summer IOP and 19 during the winter IOP) were conducted in the vicinity of the ENA site (Fig. 1).

Most G-1 flights consisted of 4 to 6 vertical profiles from near the ocean surface to about 3000 m, providing the vertical profiles of atmospheric state, trace gases, aerosol, and cloud properties in the MBL and lower free troposphere. The flights also included horizontal legs near the surface of the ocean, just below clouds, within clouds, at cloud top, and above clouds (i.e., in the lower free troposphere), with some additional porpoising legs to characterize the cloud top and inversion layers during selected flights. The horizontal legs were flown using two different patterns, with examples shown in Fig. 2. The first one was an L-shaped pattern consisting of ~ 30 km upwind and crosswind legs at different altitudes. During most of the flights employing the L-shaped pattern, the L "corner" was located above the ENA site, which is ~ 500 m from the north shore of Graciosa Island. The crosswind legs extended from the site towards the ocean (e.g., Fig. 2a) to minimize the potential influence of local emissions from the island. The 2nd type of pattern for the horizontal legs was a "Lagrangian drift", where the

Accepted for publication in *Bulletin of the American Meteorological Society.* DOI 10.1175/BAMS-D-19-0220.1.

G-1 performed crosswind stacks (i.e., the heading of G-1 was perpendicular to the wind direction) of several straight and level runs approximately 60 km in length below, within, and above cloud while drifting with the prevailing MBL wind. Measurements during the "Lagrangian drift" allow for characterization of the detailed vertical structures of the same cloud and drizzle clusters and their evolution. During four flights, the G-1 started the "Lagrangian drift" upwind of the ENA site and drifted towards the ENA site. The date, time, weather/cloud conditions, and patterns of horizontal legs for each flight are detailed in Table S2.

The ACE-ENA deployments were specifically designed to maximize the synergy between the in-situ measurements onboard the G-1 and the ongoing measurements at the ENA site, including state of the art profiling and scanning radars (Table S1). For the L-shaped G-1 flight patterns centered at the ENA site, the second generation Scanning ARM Cloud Radar (SACR-2, e.g., Kollias et al. 2016) performed crosswind and along wind Range Height Indicator (RHI) scans alternately to cover the G-1 flight path. When the G-1 performed "Lagrangian drift" legs towards the ENA site, crosswind RHI scans were performed by the SACR-2 to characterize the cloud field sampled by the G-1 as it advected over the radar (Lamer et al. 2014). In addition, the high sensitivity second generation X-band Scanning Precipitation Radar (X-SAPR2) documented the horizontal structures and variability of precipitation within a 40-km radius around the ENA site by performing several low-elevation Plan Point Indicator (PPI) scans (Lamer et al. 2019) while the vertically-pointing Ka-band Zenith Radar, laser ceilometer, and Micropulse Lidar monitored the atmospheric column over the site. To our knowledge, this is the first field campaign that combined aircraft measurements in marine low clouds with collocated high-sensitivity, scanning radar data to explore how atmospheric processes vary across MBL cloud systems with varying mesoscale organization. An example of the

Accepted for publication in *Bulletin of the American Meteorological Society.* DOI 10.1175/BAMS-D-19-0220.1.

coordination between G-1 flights and the operation of surface based remote sensing is given in the supplement and Fig S1. The summer IOP overlapped with the Azores stratoCumulus measurements Of Radiation, turbulEnce and aeroSols (ACORES) campaign, during which helicopter-borne observations of aerosols, stratocumulus microphysical and radiative properties were carried out at the ENA site (Siebert et al. 2020). The collocated measurements from ACORES provide additional synergy in advancing some of the ACE-ENA scientific objectives.

Instruments and measurements onboard the G-1 aircraft

The instruments deployed on the G-1 aircraft during ACE-ENA are listed in Table S3 (in supplement). Collectively, these instruments provide comprehensive measurements of aerosol particles, cloud droplets, and trace gas species, in addition to solar radiation, atmospheric state variables, and meteorological parameters. The mixing ratio of carbon monoxide (CO) was measured by a CO/N_2O analyzer to help identify the air mass types. An Ionicon quadrupole high-sensitivity Proton-Transfer-Reaction Mass Spectrometer (PTR-MS) was used to measure the mixing ratio of selected gas-phase volatile organic compounds, including DMS and isoprene. Particle number concentrations were measured by Condensation Particle Counters (CPCs) and aerosol size distributions were characterized by several instruments with different but overlapping size ranges, including the Fast Integrated Mobility Spectrometer (FIMS) (Kulkarni and Wang 2006; Wang et al. 2017; Wang et al. 2018) and Passive Cavity Aerosol Spectrometer Probe (PCASP). CCN concentrations were measured at two supersaturations (S = 0.14% and 0.32% during the summer IOP and S = 0.14% and 0.37% during the winter IOP). A high-resolution time-of-flight Aerosol Mass Spectrometer (HR-ToF-AMS) was deployed to measure the bulk nonrefractory aerosol composition (sulfate, nitrate, ammonium, and

Accepted for publication in *Bulletin of the American Meteorological Society.* DOI 10.1175/BAMS-D-19-0220.1.

organics). Samples collected using a Particle-Into-Liquid Sampler (PILS) were analyzed using ion chromatography to provide sub-micrometer water-soluble aerosol chemical composition (i.e., inorganics, organic acids, amines). Black carbon (BC) mass in individual particles was quantified using a Single Particle Soot Photometer (SP2). A Time-Resolved Aerosol Collector (TRAC) was deployed to collect atmospheric particles for multiple off-line post-campaign laboratory analyses (Laskin et al. 2019). The size spectrum of hydrometeors, including cloud droplets and drizzle drops, was characterized by a suite of optical probes (Table S3). A novel Holographic Detector for Clouds (HOLODEC) was deployed to sample an ensemble of hydrometeors in a localized volume (~ 20 cm^3) by digitally reconstructing interference patterns recorded by a charge-coupled device camera at 3.3 Hz (Fugal and Shaw 2009).

Two aerosol sampling inlets were used onboard the G-1 during ACE-ENA. An isokinetic inlet samples interstitial aerosol with aerodynamic diameters below 5 μm. By imposing a counterflow airstream, a counterflow virtual impactor (CVI) inlet allows only cloud droplets and large aerosol particles to be sampled. The FIMS, HR-ToF-AMS, and SP2 were switched between the isokinetic and CVI inlets, making it possible to compare the properties of cloud droplet residuals and aerosol outside of the clouds. The number concentration of nonvolatile particles was characterized by a CPC (Model 3010, TSI Inc.) downstream of a thermal denuder (Fierz et al. 2007) operated at a temperature of 300 ºC. The FIMS also periodically sampled downstream of the thermal denuder to characterize the particle size distribution of the non-volatile components.

Additional measurements at the ENA site

Accepted for publication in *Bulletin of the American Meteorological Society.* DOI 10.1175/BAMS-D-19-0220.1.

During ACE-ENA, additional aerosol measurements were carried out at the ENA site (Table S4) from June 2017 to June 2018. Aerosol size distributions from 10 to 470 nm were characterized by a scanning mobility particle sizer (SMPS). The aerosol number concentration (CN) was measured concurrently by a CPC. Both the aerosol size distribution and number concentration measurements were alternated between ambient samples and those processed by a thermal denuder operated at 300ºC every 4 minutes. The activated fraction of size selected particles as a function of supersaturation was measured using a system that consists of a Differential Mobility Analyzer (DMA, TSI Inc., Model 3081) coupled to a CPC (TSI Inc., Model 3010) and a CCN counter (CCNC, Droplet Measurement Technologies, Boulder, CO) (Mei et al. 2013b; Thalman et al. 2017). The activated fraction allows for the derivation of the particle hygroscopicity parameter under supersaturated conditions (κ_{CCN}) (Petters and Kreidenweis 2007; Mei et al. 2013a; Wang et al. 2019a).

Meteorological conditions

The Azores are largely dominated by the North Atlantic Oscillation, which is comprised of the semi-permanent Azores high and Icelandic low (Cropper et al. 2015; Wood et al. 2015). During the summer IOP (Fig. 3a), the Azores high is the dominant feature in the Atlantic and is commonly located to southwest of the Azores (Wood et al. 2015; Mechem et al. 2018). The Icelandic low is diminished and often broken into smaller circulations. During the winter IOP (Fig. 3b), the center of the Azores high shifts to the eastern Atlantic and is primarily located directly over the Azores. Compared to the winter IOP, the midlatitude cyclone tracks during the summer IOP are further north, with less-frequent frontal passages across the Azores, as indicated by the smaller standard deviations in mean sea level pressure (MSLP). These mean

Accepted for publication in *Bulletin of the American Meteorological Society.* DOI 10.1175/BAMS-D-19-0220.1.

structures are largely consistent with the 32-year climatology calculated from reanalysis (Fig. 2a,b in Wood et al. 2015). However, while the Azores high is climatologically stronger during the summer than the winter (Hasanean 2004, Wood et al. 2015), the opposite was observed during the two IOPs with the average MSLP being 5 hPa higher during the winter. The Icelandic low deepens during the winter and is associated with a higher frequency of midlatitude cyclone tracks of which many contain frontal systems that extend south to the Azores, as indicated by the higher standard deviation in MSLP. During the winter IOP particularly near the end of January, as midlatitude cyclones tracked eastward over the north Atlantic, the cyclones became occluded near Iceland and the cold fronts associated with these systems would lose upper-level support and stall over the Azores.

Surface conditions at the ENA site (Fig. 4a) indicate more frequent high MSLP during the winter IOP, with a median MSLP of 1031.5 hPa and 1024.5 hPa during the winter and summer, respectively. The wider spread in MSLP during the winter IOP is generated by passing frontal systems. Distributions in temperature (dew point temperature) are relatively similar between both IOPs, but offset by around 6.5˚C (6.2˚C; Fig. 4b,c). Distributions of surface RH values are also similar, with the winter IOP having a higher frequency of RH values below 65% (Fig. 4d). Surface winds typically range from southwest to northeast during the summer IOP and are typically directly out of the southwest or northeast during the winter IOP, which are consistent with climatology (Fig. 2c,d in Wood et al. 2015) except for the high frequency of northeasterly winds during the winter (Fig. 4e,f). Stronger winds are also present during the winter, with wind speeds surpassing 9 m s^{-1} 33% of the time as compared to 20% during the summer.

Temperature and RH profiles taken by soundings launched from the ENA site showcase the variability of the boundary layer across the summer and winter IOPs (Fig. 5a-d). During the first half of the summer IOP, on-site observers noted stratocumulus cloud layers that

Accepted for publication in *Bulletin of the American Meteorological Society.* DOI 10.1175/BAMS-D-19-0220.1.

developed were often very thin and rapidly dissipated after sunrise (not shown), resulting in lower cloud fraction (Fig. 5e,g). The first half of the IOP was characterized by a lack of well-defined inversions (Fig. 5a,c), with unbroken overcast stratocumulus becoming more prevalent only later in the period. The winter IOP contained more consistent stratocumulus conditions (Fig. 5f,h) and regularly exhibited a well-defined boundary layer, with sharper gradients in RH across the boundary-layer top that corresponded with stronger inversions (Fig. 5b,d).

Observations and early findings

In this section, we highlight some of the observations and early findings from the ACE-ENA in the four key topic areas described above.

Aerosol properties and processes in the remote MBL

The MBL in the ENA is often decoupled into two sublayers (i.e., a surface mixed layer above the ocean surface and an upper decoupled layer), especially following the passage of cold fronts, when strong convective activities often lead to deeper boundary layers. Using the airborne measurements during ACE-ENA, Zheng et al. (2020b) show that new particle formation takes place in the upper decoupled layer following the passage of cold fronts, when open-cell convection and scattered cumulus clouds frequently occur. The new particle formation is due to the combination of low existing aerosol surface area, cold air temperature, availability of reactive gases, and high actinic fluxes in the clear regions between scattered cumulus clouds. As the new particle formation occurs aloft in the upper MBL, it could not be directly observed in earlier studies based on surface measurements alone (e.g., Bates et al. 1998). The new particles formed in the upper part of the MBL are mixed down to the surface

Accepted for publication in *Bulletin of the American Meteorological Society.* DOI 10.1175/BAMS-D-19-0220.1.

layer, where they can grow through condensation. The year-long aerosol size distribution measurements at the ENA site frequently show continuous growth of nucleation mode particles with initial mode diameter below 20 nm, suggesting such new particle formation occurs frequently, and that the growth of the new particles helps replenish aerosol and CCN in the remote MBL following the passage of cold fronts (Zheng et al. 2020b). Given the high susceptibility of marine low clouds, the new particle formation inside the MBL and its impact on CCN population need to be further studied.

The large number of flights allows for statistical characterization of the vertical profiles of aerosol properties and their variations between the two seasons (Wang et al. 2021). Here particles that are too small to form cloud droplets under the average cloud supersaturation inside the MBL (i.e., particles below the Hoppel minimum) are referred to as "pre-CCN". On average, concentrations of CCN (N_{CCN}), pre-CCN particles ($N_{\text{pre-CCN}}$), and particles larger than ($N_{>10}$) all exhibit higher values during the summer than the winter in both the MBL and lower free troposphere (Fig. 6a-c). During the summer, at an altitude of ~ 2000 m, average N_{CCN} and mass concentrations of BC (m_{BC}) and organics (m_{org}) are substantially higher than their corresponding median values, indicating periods of abnormally high N_{CCN}, m_{BC}, and m_{org} in the lower free troposphere (Fig. 6c, 6e, and 6f). As there is no substantial source of BC in the lower free troposphere over the open ocean, the abnormally high N_{CCN}, m_{BC}, and m_{org} are attributed to long-range transported aerosol layers deriving from continental emissions. The sources of the aerosol in these free troposphere layers include both biomass burning and pollution from North America (e.g., Zheng et al. 2020c; Zawadowicz et al. 2021), with the contribution of pollution likely being the dominant one (Wang et al. 2021). On average, N_{CCN} in the lower free troposphere is slightly lower than that in the MBL, suggesting that entrainment of free troposphere air does not serve as a direct source of CCN in the MBL. However, in both

Accepted for publication in *Bulletin of the American Meteorological Society.* DOI 10.1175/BAMS-D-19-0220.1.

seasons, entrainment of free troposphere air is a major source of pre-CCN particles (i.e., nucleation/Aitken mode particles) in the MBL due to much elevated $N_{\text{pre-CCN}}$ in the lower free troposphere (Fig. 6b).

Once the pre-CCN particles are entrained into the MBL, they can reach CCN size ranges through condensational growth (Zheng et al. 2018; Zheng et al. 2020a). Therefore, free troposphere entrainment represents an important, but "indirect" source of CCN in the midlatitude MBL. The higher MBL N_{CCN} during the summer is partially due to the increased condensational growth rate of Aitken mode particles as a result of stronger oceanic emissions of volatile organic compounds including DMS (Zawadowicz et al. 2021). Zheng et al. (2020a) derived the hygroscopicity of condensing species during particle growth events from the size-resolved particle activated fraction measured at the ENA site. By taking advantage of the contrasting hygroscopicities between sulfate and secondary organics, they showed that organics represent important or even the dominant condensing species during ~80% of growth events. The secondary organic species likely derive from a variety of precursors, including isoprene, monoterpenes, and aliphatic amines related to marine biogenic activity (e.g., Willis et al. 2017; Mayer et al. 2020) and those produced by the oxidation reactions at the air–sea interface, such as organic acids (Mungall et al. 2017). The higher precipitation rates in the winter campaign (Fig. 8, discussed in the next section) likely leads to increased coalescence scavenging of CCN and thus contributes to the seasonal variation of N_{CCN} in the MBL. The vertical profile of sulfate mass concentration indicates a surface source in both seasons (Fig. 6d), consistent with the picture that over open oceans, sulfate in submicron aerosol is mostly derived from DMS through both gas phase and in-cloud oxidations (Ovadnevaite et al. 2014).

Aerosol impacts on cloud microphysics and precipitation

Accepted for publication in *Bulletin of the American Meteorological Society*. DOI 10.1175/BAMS-D-19-0220.1.

The strong summertime maximum in CCN concentration discussed above was noted during an earlier deployment at Graciosa Island in 2009/10 (Wood et al. 2015). ACE-ENA provides the first in-situ measurements in the region showing correspondingly higher N_d on average. Intriguingly, the ratio of the mean summer to winter N_d (~1.5) is much lower than the seasonal ratio of accumulation mode aerosol concentration (N_{Acc}) in the surface mixed layer inferred from the PCASP number (~2.9) and CCN concentration (N_{CCN}, ~2.9) measurements. Figure 7 shows that the relationship between N_d and N_{Acc} is seasonally dependent, with a much steeper slope in winter than in summer. Thus, a higher fraction of the accumulation mode particles is being activated in winter than in summer, which helps dampen the seasonal cycle in N_d. For a fixed updraft speed, higher aerosol concentrations lead to lower peak supersaturations and lower activation fractions due to competition for water vapor, which could partly explain the damped seasonal cycle of N_d compared with N_{CCN} or N_{Acc}. However, this is certainly not the sole reason for the greater "activation efficiency" in winter. Results from the turbulence measurements on the G-1 indicate that updrafts tend to be stronger in winter on average (Wyant et al., 2020). Further, vertical profiles from the G-1 indicate that the MBL is more decoupled during the summer than the winter, which results in stronger aerosol stratification in summer. On average, N_{Acc} decreases with height in the MBL in a similar manner as N_{CCN} (see Fig. 6c), but the decrease is more pronounced in summer. Most MBL clouds reside in and activate aerosol primarily from the upper MBL. The greater stratification and weaker updraft speed serve to dampen the seasonal cycle of N_d compared with the cycles of surface N_{Acc} and N_{CCN} (Wyant et al. 2020).

Although the seasonal N_d cycle is weaker than that in N_{CCN}, an important question is whether wintertime low clouds precipitate more readily than summertime clouds, as would be expected from prior assessments of the sensitivity of warm rain to CCN (Sorooshian et al.

Accepted for publication in *Bulletin of the American Meteorological Society.* DOI 10.1175/BAMS-D-19-0220.1.

2010; Terai et al. 2012; Mann et al. 2014). We find that for intermediate precipitation rates (0.1-10 mm day^{-1}), there is a shift toward higher precipitation rates in the winter IOP (Fig. 8), with little difference in the frequency of the heaviest precipitation rates. Liquid water path (LWP) distributions at the ENA site (not shown) are similar between summer and winter, leaving the potential for the seasonality in precipitation to be driven by the seasonal N_d and aerosol contrasts. However, synoptic forcing differences between winter and summer play a role at modulating low cloud properties and the condensate distributions, so controlling for synoptic regime (e.g., using self-organizing maps, Mechem et al., 2018) will be required to appropriately account for seasonal synoptic variability before a definitive assessment of the role of aerosols in the seasonal cycle of warm rain over the Azores.

Cloud Microphysical and Macrophysical Structures, and Turbulent Entrainment Mixing Processes

The effect of entrainment-mixing on droplet size spectrum appears to be dependent on the sampling scales (Burnet and Brenguier 2007; Lu et al. 2014; Beals et al. 2015; Kumar et al. 2018). Gao et al. (2020) analyzed in-situ ACE-ENA data and found two opposite trends of scale dependency: entrainment mixing can become more homogeneous or more inhomogeneous with increasing averaging scales, depending on the properties of the entrained dry air, cloud microphysics, and turbulence. Addressing this perplexing issue requires measurements at centimeter scales from the HOLODEC deployed during ACE-ENA (Fig. S2), and is a topic of ongoing research.

The effect of entrainment-mixing on droplet size spectrum can also vary vertically. Most previous studies showed that entrainment-mixing appears to be more homogeneous with

Accepted for publication in *Bulletin of the American Meteorological Society.* DOI 10.1175/BAMS-D-19-0220.1.

decreasing altitude, attributed to more pronounced droplet evaporation in cloud parcels with lower liquid water content (i.e., cloud parcels that are more strongly influenced by entrainment mixing) as the cloud parcels descend from cloud top (Wang et al. 2009; Yum et al. 2015). Such vertical trend is also evident during some of the ACE-ENA flights (Yeom et al. 2020). Figure 9 shows an example of such behavior examined in a new type of mixing diagram composed of the two axes, $\mathrm{Log}_{10}L$ and $\mathrm{Log}_{10}\tau_p$, where L is cloud droplet liquid water content and τ_p is the phase relaxation time, which represents the time required to restore saturation in the entrainment-affected and subsaturated parcel by evaporation of cloud droplets (Yeom et al. 2020). The relationship between $\mathrm{Log}_{10}L$ and $\mathrm{Log}_{10}\tau_p$ indicates extreme inhomogeneous mixing near cloud top (Fig. 9a), whereas the mixing appears more homogeneous in the mid-level of the cloud layer (Fig. 9b). In stratiform clouds, entrainment occurs primarily at the top of the clouds owing to cloud-top radiative and/or evaporative cooling (Wood 2012). The vertical variation of the entrainment-mixing process may also be related to the vertical variation of the RH of engulfed clear air parcels (i.e., eddies), which is expected to increase as the parcels move downward and mix with cloudy air. The mixing of engulfed clear air with cloudy air and the subsequent evaporation of cloud droplets increase the RH of the clear air parcel, until the parcel becomes saturated and the clear air parcel "disappears". All else being equal, a higher RH results in a longer time required for the droplets to evaporate and thus would favor a transition to more homogeneous mixing with increasing distance below cloud top. However, some nonprecipitating stratiform clouds sampled during ACE-ENA exhibited an unusual increase in the homogeneous mixing degree (ψ) (Lu et al. 2013b) with height, and an example from the flight on June 28, 2017 is given in Fig. 10a. This opposite trend is generally consistent with the vertical profiles of D_a (Fig. 10a) and the transition scale number (N_L, Fig. 10a), which is defined as the ratio of the transition length scale (L^*) (Lehmann et al. 2009) to the Kolmogorov length

Accepted for publication in *Bulletin of the American Meteorological Society.* DOI 10.1175/BAMS-D-19-0220.1.

scale (η) (Lu et al. 2011). The vertical profiles support the notion that the specific entrainment-mixing process is determined by the relative role of turbulent mixing time versus the droplet evaporation time and due primarily to the increase with height of turbulent dissipation rate (ε) and droplet sizes (Fig. 10b). However, clear air parcels, which originate from entrained dry air, exhibit increasing sizes with altitude, leading to longer turbulent mixing time near cloud top and thus favoring the opposite trend (i.e., more heterogenous mixing near cloud top).

In addition to the entrainment mixing, the sub-grid scale horizontal variations of cloud water content and N_d, the covariance between them, and the implications for the parameterized autoconversion rate in global climate models were examined using ACE-ENA measurements (Zhang et al. 2020). Chiu et al. (2021) introduced new parameterizations of autoconversion and accretion rates using machine learning techniques and in-situ measurements during ACE-ENA. They also discovered a key role of drizzle number concentration in predicting autoconversion rates, which is supported by theory and should be also considered in future parameterizations.

Evaluation of remote sensing retrievals

The ACE-ENA campaign provided high-quality collocated in-situ measurements that are essential for evaluating and advancing remote sensing techniques for drizzling clouds. Wu et al. (2020) retrieved concurrent cloud and drizzle microphysical properties using measurements of lidar, Ka-band zenith pointing cloud radar, and microwave radiometer (MWR) during the ACE-ENA campaign. Evaluations against in-situ cloud probe measurements show that the associated median errors of their retrieval are in the order of magnitude of 15%–50%. In this type of synergistic retrieval methods, active sensors play a key role in providing information

Accepted for publication in *Bulletin of the American Meteorological Society.* DOI 10.1175/BAMS-D-19-0220.1.

on the profiles of cloud and drizzle drop size, while passive sensors are crucial for constraining cloud column properties, such as LWP.

Similarly, the Ensemble Cloud Retrieval method (ENCORE) described in Fielding et al. (2015) also relies on lidar and Ka-band cloud radar, but it uses shortwave zenith radiance measurements to constrain cloud optical depth. This allows us to use MWR observations as an independent dataset for additional evaluations, as detailed below. Figure 11 shows an example from 18 July 2017 with a persistent stratocumulus deck. For cloud properties, the ENCORE-retrieved LWP agrees well with those from MWR observations at the ENA site (Fig. 12); the associated RMSE is about 33 g m^{-2}, comparable to the uncertainty in MWR retrievals (Crewell and Lohnert 2003). The retrieved cloud droplet number concentration appears consistent with in-situ observations at 0.5–1 km altitude (Fig. 13a), mainly ranging between 40–80 cm^{-3}. The in-situ data also show an increase in cloud effective radius and water content with height, though the water content has a decrease at cloud tops. Overall, the agreement between in-situ data and the ENCORE retrieval tends to be better in the middle of cloud layers at 0.75–1 km than near cloud bases and cloud tops (Fig. 13a–c).

We used cloud probe measurements from 50 to 500 μm in diameter to evaluate ENCOR drizzle properties. Figures 13d–f show that the retrieved number concentrations follow a similar vertical structure to observations, ranging mainly between 0.01 and 0.1 cm^{-3}. The agreement in drizzle effective radius and water content is good in the lower part of clouds, considering the large spatial and temporal variability of drizzle fields. However, while the retrieved drizzle drop size and water content decrease with height, consistent with our conceptual model that drizzle drops become bigger via accretion when they fall through the cloud layer, the in-situ observations show an opposite gradient. This opposite behavior is likely due to the strong sensitivity to the cut-off threshold used in in-situ data for defining the

Accepted for publication in *Bulletin of the American Meteorological Society.* DOI 10.1175/BAMS-D-19-0220.1.

maximum drizzle size, but also possibly due to sampling issues. Although further examinations of the entire campaign dataset are necessary to ensure that an appropriate cut-off is used and that the intercomparison is meaningful, these preliminary results are encouraging and highlight a crucial step forward in better characterizing concurrent cloud and drizzle properties from remote sensing observations.

Summary and outlook

The large number of ACE-ENA flights provided comprehensive characterizations of boundary layer and lower free troposphere structures and associated vertical distributions and horizontal variations of low clouds and aerosols in the Azores under representative meteorological conditions. Already, analyses of the ACE-ENA data have advanced our understanding of the processes driving MBL CCN concentrations, seasonal variations of cloud and drizzle properties, and the effect of entrainment mixing on cloud microphysics. The in-situ ACE-ENA measurements have allowed for the evaluation of retrieval algorithms for ground-based remote sensing. Together with the long-term observations at the ENA site, the comprehensive datasets collected during ACE-ENA will enable a more holistic and complete understanding of the controlling processes for MBL CCN population, cloud lifecycle, and the interactions among aerosol, clouds, and precipitation. Following are a sampling of the scientific objectives that can be addressed in ongoing and future studies:

(1) Developing the budget of the CCN population in the remote MBL and the variation of different budget terms with both season and synoptic conditions. These budget terms include the contributions from different sources (e.g., new particle formation, entrainment of free troposphere air, production of sea spray aerosol, and growth of pre-CCN particles), and removal by various processes (e.g., coalescence scavenging).

Accepted for publication in *Bulletin of the American Meteorological Society.* DOI 10.1175/BAMS-D-19-0220.1.

(2) Evaluating key processes controlling the MBL CCN budget using LES models with fully interactive aerosol processing, including an assessment of the role played by pre-CCN particles.

(3) Evaluating the representation of aerosol properties, their vertical profiles and temporal variability over different seasons and synoptic conditions in global climate models using the ACE-ENA measurements and long-term ENA observations. Through model sensitivity experiments the causes for the model biases would be examined and the representation of the key aerosol processes be improved.

(4) Quantifying the role of aerosol in the seasonal cycle of warm rain in the ENA. The analysis will employ a statistical approach to separate effects of cloud microphysics from macrophysical controls on precipitation by taking advantage of (1) the measurements from the large number of ACE-ENA flights, and (2) cloud/drizzle vertical profiles retrieved from long-term surface based remote sensing using algorithms validated by ACE-ENA in-situ measurements.

(5) Investigating the variations of the entrainment mixing process with spatial scale and altitude by examining the cloud microphysical relationships using both the measurements from conventional probes and centimeter scale measurements from HOLODEC.

(6) Examining the relationship between entrainment-mixing process and spectral shape of cloud droplet size distributions, investigating the entrainment rate near cloud top and factors affecting the entrainment rate, and examining the comprehensive thermodynamics-dynamics-microphysics connections by combining in-situ measurements and cloud structures retrieved from surface based remote sensing.

Accepted for publication in *Bulletin of the American Meteorological Society.* DOI 10.1175/BAMS-D-19-0220.1.

(7) Providing cloud process rates in warm rain formation by applying advanced retrieval methods to long-term ENA observations, for improving our process-level understanding and model prediction of drizzle frequency and amount.

Acknowledgments.

The ACE-ENA campaign would not have been successful without the contributions of many individuals including the G-1 flight, ground, and instrument support crew (M. Hubbell, C. Eveland, J. Ray, J. Hubbe, M. Crocker, P. Carroll, F. Reis, A. Mendoza, D. Nelson, M. Newburn, and W. Irvin), the ENA site staff (P. Ortega, C. Sousa, B. Cunha, and T. Silva), Field Instrument and Operation (FIDO) staff at Los Alamos National Laboratory (K. Nitschke, and H. Powers), and other participating scientists (Nitin Bharadwaj, Bradley Isom, Jennifer Kafka, and Stephen Springston). We acknowledge the support from the Government of the Autonomous Region of the Azores, the Minister of Science of Portugal, and the Air Force of Portugal through the Command of the Air Space of the Azores, command and all the air force staff of Airbase Nº 4 (Lajes). The ACE-ENA field campaign was supported by the Atmospheric Radiation Measurement (ARM) Climate Research Facility and the Environmental Molecular Sciences Laboratory (EMSL), both are U.S. Department of Energy (DOE) Office of Science User Facilities sponsored by the Office of Biological and Environmental Research. We thank Dr. Tamara Pinterich for her help in the preparation and deployment of the FIMS onboard the G-1 aircraft during ACE-ENA. The research was supported by the Atmospheric System Research (ASR) program as part of the DOE Office of Biological and Environmental Research under award Nos. DE-SC0020259 (J. Wang), DE-SC0012704 (BNL), DE–SC0016522 (D. Mechem), DE-SC0021167 (C. Chiu), DE-SC0018948 (A. Laskin and R. Moffet), DE-SC0016370 (D. Knopf), KP1701000/57131 (J. Shilling and M. Zawadowicz), DE-AC02-

Accepted for publication in *Bulletin of the American Meteorological Society.* DOI 10.1175/BAMS-D-19-0220.1.

06CH11357 (V. Ghate), and DE-SC0020053 (R. Shaw). S. S. Yum and J. Yeom acknowledge the support of Korea Meteorological Administration Research and Development Program under Grant KMI2018-03511. Chunsong Lu and Sinan Gao were supported by the National Natural Science Foundation of China (41822504). Xiquan Dong was supported by the NSF project under grant AGS-2031751 and as part of the "Enabling Aerosol-cloud interactions at GLobal convection-permitting scalES (EAGLES)" project (74358), funded by the U.S. Department of Energy, Office of Biological and Environmental Research, Earth System Modeling program with a subcontract to the University of Arizona. Part of the abstract was published by American Geophysical Union 2017 Fall conference.

Data Availability Statement.

All data used in this study are available at Atmospheric Radiation Measurement (ARM) Climate Research Facility data archive https://www.arm.gov/research/campaigns/aaf2017ace-ena.

Accepted for publication in *Bulletin of the American Meteorological Society*. DOI 10.1175/BAMS-D-19-0220.1.

REFERENCES

Ackerman, A. S., M. P. Kirkpatrick, D. E. Stevens, and O. B. Toon, 2004: The impact of humidity above stratiform clouds on indirect aerosol climate forcing. *Nature*, **432,** 1014-1017, doi: 10.1038/nature03174.

Albrecht, B., M. Fang, and V. Ghate, 2016: Exploring Stratocumulus Cloud-Top Entrainment Processes and Parameterizations by Using Doppler Cloud Radar Observations. *J. Atmos. Sci.*, **73,** 729-742, doi: 10.1175/jas-d-15-0147.1.

Albrecht, B. A., 1989: Aerosols, cloud microphysics, and fractional cloudiness. *Science*, **245,** 1227-1230.

Baker, M. B., R. G. Corbin, and J. Latham, 1980: The influence of entrainment on the evolution of cloud droplet spectra .1. a model of inhomogeneous mixing. *Q. J. R. Meteorol. Soc.*, **106,** 581-598.

Bates, T. S., and Coauthors, 1998: Processes controlling the distribution of aerosol particles in the lower marine boundary layer during the First Aerosol Characterization Experiment (ACE 1). *J. Geophys. Res.*, **103,** 16369-16383, doi: 10.1029/97jd03720.

Beals, M. J., J. P. Fugal, R. A. Shaw, J. Lu, S. M. Spuler, and J. L. Stith, 2015: Holographic measurements of inhomogeneous cloud mixing at the centimeter scale. *Science*, **350,** 87-90, doi: 10.1126/science.aab0751.

Bellouin, N., and Coauthors, 2020: Bounding Global Aerosol Radiative Forcing of Climate Change. *Rev. Geophys.*, **58**, doi: 10.1029/2019rg000660.

Bodas-Salcedo, A., J. P. Mulcahy, T. Andrews, K. D. Williams, M. A. Ringer, P. R. Field, and G. S. Elsaesser, 2019: Strong Dependence of Atmospheric Feedbacks on Mixed-Phase Microphysics and Aerosol-Cloud Interactions in HadGEM3. *Journal of Advances in Modeling Earth Systems*, **11,** 1735-1758, doi: 10.1029/2019ms001688.

Bony, S., and J. L. Dufresne, 2005: Marine boundary layer clouds at the heart of tropical cloud feedback uncertainties in climate models. *Geophys. Res. Lett.*, **32**, doi: 10.1029/2005gl023851.

Bretherton, C. S., 2015: Insights into low-latitude cloud feedbacks from high-resolution models. *Philosophical Transactions of the Royal Society a-Mathematical Physical and Engineering Sciences*, **373**, doi: 10.1098/rsta.2014.0415.

Brüggemann, M., N. Hayeck, and C. George, 2018: Interfacial photochemistry at the ocean surface is a global source of organic vapors and aerosols. *Nature Communications*, **9,** 2101, doi: 10.1038/s41467-018-04528-7.

Burnet, F., and J. L. Brenguier, 2007: Observational study of the entrainment-mixing process in warm convective clouds. *J. Atmos. Sci.*, **64,** 1995-2011.

Cadeddu, M. P., V. P. Ghate, and M. Mech, 2020: Ground-based observations of cloud and drizzle liquid water path in stratocumulus clouds. *Atmos. Meas. Tech.*, **13,** 1485-1499, doi: 10.5194/amt-13-1485-2020.

Carslaw, K. S., and Coauthors, 2013: Large contribution of natural aerosols to uncertainty in indirect forcing. *Nature*, **503,** 67-71, doi: 10.1038/nature12674.

Accepted for publication in *Bulletin of the American Meteorological Society*. DOI 10.1175/BAMS-D-19-0220.1.

Charlson, R. J., J. E. Lovelock, M. O. Andreae, and S. G. Warren, 1987: Oceanic phytoplankton, atmospheric sulphur, cloud albedo and climate. *Nature*, **326,** 655-661, doi: 10.1038/326655a0.

Chen, Y. C., L. Xue, Z. J. Lebo, H. Wang, R. M. Rasmussen, and J. H. Seinfeld, 2011: A comprehensive numerical study of aerosol-cloud-precipitation interactions in marine stratocumulus. *Atmos. Chem. Phys.*, **11,** 9749-9769, doi: 10.5194/acp-11-9749-2011.

Chen, Y. C., M. W. Christensen, L. Xue, A. Sorooshian, G. L. Stephens, R. M. Rasmussen, and J. H. Seinfeld, 2012: Occurrence of lower cloud albedo in ship tracks. *Atmos. Chem. Phys.*, **12,** 8223-8235, doi: 10.5194/acp-12-8223-2012.

Chiu, J. C., and Coauthors, 2021: Observational constraints on warm cloud microphysical processes using machine learning and optimization techniques. *Geophys. Res. Lett.*, **48**, doi: 10.1029/2020GL091236.

Christensen, M. W., and G. L. Stephens, 2011: Microphysical and macrophysical responses of marine stratocumulus polluted by underlying ships: Evidence of cloud deepening. *J. Geophys. Res.*, **116**, doi: 10.1029/2010jd014638.

Clarke, A. D., J. L. Varner, F. Eisele, R. L. Mauldin, D. Tanner, and M. Litchy, 1998: Particle production in the remote marine atmosphere: Cloud outflow and subsidence during ACE 1. *J. Geophys. Res.*, **103,** 16397-16409, doi: 10.1029/97jd02987.

Coakley, J. A., and C. D. Walsh, 2002: Limits to the aerosol indirect radiative effect derived from observations of ship tracks. *J. Atmos. Sci.*, **59,** 668-680, doi: 10.1175/1520-0469(2002)059<0668:lttair>2.0.co;2.

Crewell, S., and U. Lohnert, 2003: Accuracy of cloud liquid water path from ground-based microwave radiometry - 2. Sensor accuracy and synergy. *Radio Science*, **38**, doi: 10.1029/2002rs002634.

Cropper, T., E. Hanna, M. A. Valente, and T. Jonsson, 2015: A daily Azores-Iceland North Atlantic Oscillation index back to 1850. *Geoscience Data Journal*, **2,** 12-24, doi: 10.1002/gdj3.23.

Feingold, G., and H. Siebert, 2009: Cloud-Aerosol Interactions from the Micro to the Cloud Scale. *Clouds in the Perturbed Climate System: Their Relationship to Energy Balance, Atmospheric Dynamics, and Precipitation***,** 319-338.

Feingold, G., S. M. Kreidenweis, B. Stevens, and W. R. Cotton, 1996: Numerical simulations of stratocumulus processing of cloud condensation nuclei through collision-coalescence. *J. Geophys. Res.*, **101,** 21391-21402, doi: 10.1029/96jd01552.

Feingold, G., W. L. Eberhard, D. E. Veron, and M. Previdi, 2003: First measurements of the Twomey indirect effect using ground-based remote sensors. *Geophys. Res. Lett.*, **30**, doi: 10.1029/2002gl016633.

Fielding, M. D., J. C. Chiu, R. J. Hogan, G. Feingold, E. Eloranta, E. J. O'Connor, and M. P. Cadeddu, 2015: Joint retrievals of cloud and drizzle in marine boundary layer clouds using ground-based radar, lidar and zenith radiances. *Atmos. Meas. Tech. Discuss.*, **8,** 1833-1889.

Fierz, M., M. G. C. Vernooij, and H. Burtscher, 2007: An improved low-flow thermodenuder. *J Aerosol Sci*, **38,** 1163-1168, doi: https://doi.org/10.1016/j.jaerosci.2007.08.006.

Accepted for publication in *Bulletin of the American Meteorological Society*. DOI 10.1175/BAMS-D-19-0220.1.

Frossard, A. A., L. M. Russell, S. M. Burrows, S. M. Elliott, T. S. Bates, and P. K. Quinn, 2014: Sources and composition of submicron organic mass in marine aerosol particles. *J. Geophys. Res.*, **119,** 12977-13003, doi: 10.1002/2014jd021913.

Fugal, J. P., and R. A. Shaw, 2009: Cloud particle size distributions measured with an airborne digital in-line holographic instrument. *Atmos. Meas. Tech.*, **2,** 259-271, doi: 10.5194/amt-2-259-2009.

Gao, S. N., C. S. Lu, Y. G. Liu, F. Mei, J. Wang, L. Zhu, and S. Q. Yan, 2020: Contrasting Scale Dependence of Entrainment-Mixing Mechanisms in Stratocumulus Clouds. *Geophys. Res. Lett.*, **47**, doi: 10.1029/2020gl086970.

Gerber, H., 1996: Microphysics of marine stratocumulus clouds with two drizzle modes. *J. Atmos. Sci.*, **53,** 1649-1662, doi: 10.1175/1520-0469(1996)053<1649:momscw>2.0.co;2.

Gerber, H., G. Frick, S. P. Malinowski, J. L. Brenguier, and F. Burnet, 2005: Holes and entrainment in stratocumulus. *J. Atmos. Sci.*, **62,** 443-459, doi: 10.1175/jas-3399.1.

Gettelman, A., H. Morrison, C. R. Terai, and R. Wood, 2013: Microphysical process rates and global aerosol-cloud interactions. *Atmos. Chem. Phys.*, **13,** 9855-9867, doi: 10.5194/acp-13-9855-2013.

Giangrande, S. E., D. Wang, M. J. Bartholomew, M. P. Jensen, D. B. Mechem, J. C. Hardin, and R. Wood, 2019: Midlatitude Oceanic Cloud and Precipitation Properties as Sampled by the ARM Eastern North Atlantic Observatory. *J. Geophys. Res.*, **124,** 4741-4760, doi: 10.1029/2018jd029667.

Hoffmann, F., and G. Feingold, 2019: Entrainment and Mixing in Stratocumulus: Effects of a New Explicit Subgrid-Scale Scheme for Large-Eddy Simulations with Particle-Based Microphysics. *J. Atmos. Sci.*, **76,** 1955-1973, doi: 10.1175/jas-d-18-0318.1.

Hudson, J. G., and S. S. Yum, 2001: Maritime-continental drizzle contrasts in small cumuli. *J. Atmos. Sci.*, **58,** 915-926, doi: 10.1175/1520-0469(2001)058<0915:mcdcis>2.0.co;2.

IPCC, 2013: *Climate Change 2013: The Physical Science Basis: Contribution of Working Group I to the Fourth Assessment Report of the Intergovernmental Panel on Climate Change.* Cambridge University Press.

Joshil, S. S., C. M. Nguyen, V. Chandrasekar, J. C. Chiu, and Y. Blanchard, 2020: Separating Cloud and Drizzle Signals in Radar Doppler Spectra Using a Parametric Time Domain Method. *J. Atmos. Oceanic Technol.*, **37,** 1669-1680, doi: 10.1175/jtech-d-20-0061.1.

Kollias, P., and Coauthors, 2016: Development and Applications of ARM Millimeter-Wavelength Cloud Radars. *Meteorological Monographs*, **57,** 17.11-17.19, doi: 10.1175/amsmonographs-d-15-0037.1.

Kooperman, G. J., M. S. Pritchard, and R. C. J. Somerville, 2013: Robustness and sensitivities of central US summer convection in the super-parameterized CAM: Multi-model intercomparison with a new regional EOF index. *Geophys. Res. Lett.*, **40,** 3287-3291, doi: 10.1002/grl.50597.

Kulkarni, P., and J. Wang, 2006: New fast integrated mobility spectrometer for real-time measurement of aerosol size distribution - I: Concept and theory. *J. Aerosol Sci.*, **37,** 1303-1325.

Accepted for publication in *Bulletin of the American Meteorological Society.* DOI 10.1175/BAMS-D-19-0220.1.

Kumar, B., P. Gotzfried, N. Suresh, J. Schumacher, and R. A. Shaw, 2018: Scale Dependence of Cloud Microphysical Response to Turbulent Entrainment and Mixing. *Journal of Advances in Modeling Earth Systems*, **10,** 2777-2785, doi: 10.1029/2018ms001487.

L'Ecuyer, T. S., W. Berg, J. Haynes, M. Lebsock, and T. Takemura, 2009: Global observations of aerosol impacts on precipitation occurrence in warm maritime clouds. *J. Geophys. Res.*, **114**, doi: 10.1029/2008jd011273.

Lamer, K., A. Tatarevic, I. Jo, and P. Kollias, 2014: Evaluation of gridded scanning ARM cloud radar reflectivity observations and vertical doppler velocity retrievals. *Atmos. Meas. Tech.*, **7,** 1089-1103, doi: 10.5194/amt-7-1089-2014.

Lamer, K., B. P. Treserras, Z. Zhu, B. Isom, N. Bharadwaj, and P. Kollias, 2019: Characterization of shallow oceanic precipitation using profiling and scanning radar observations at the Eastern North Atlantic ARM observatory. *Atmos. Meas. Tech.*, **12,** 4931-4947, doi: 10.5194/amt-12-4931-2019.

Laskin, A., R. C. Moffet, and M. K. Gilles, 2019: Chemical Imaging of Atmospheric Particles. *Accounts of Chemical Research*, **52,** 3419-3431, doi: 10.1021/acs.accounts.9b00396.

Lehmann, K., H. Siebert, and R. A. Shaw, 2009: Homogeneous and Inhomogeneous Mixing in Cumulus Clouds: Dependence on Local Turbulence Structure. *J. Atmos. Sci.*, **66,** 3641–3659.

Lohmann, U., and J. Feichter, 2005: Global indirect aerosol effects: a review. *Atmos. Chem. Phys.*, **5,** 715-737.

Lolli, S., E. J. Welton, and J. R. Campbell, 2013: Evaluating Light Rain Drop Size Estimates from Multiwavelength Micropulse Lidar Network Profiling. *J. Atmos. Oceanic Technol.*, **30,** 2798-2807, doi: 10.1175/jtech-d-13-00062.1.

Lu, C. S., Y. G. Liu, and S. J. Niu, 2011: Examination of turbulent entrainment-mixing mechanisms using a combined approach. *J. Geophys. Res.*, **116**, doi: 10.1029/2011jd015944.

Lu, C. S., S. J. Niu, Y. G. Liu, and A. M. Vogelmann, 2013a: Empirical relationship between entrainment rate and microphysics in cumulus clouds. *Geophys. Res. Lett.*, **40,** 2333-2338, doi: 10.1002/grl.50445.

Lu, C. S., Y. G. Liu, S. J. Niu, and S. S. Endo, 2014: Scale dependence of entrainment-mixing mechanisms in cumulus clouds. *J. Geophys. Res.*, **119,** 13877-13890, doi: 10.1002/2014jd022265.

Lu, C. S., Y. G. Liu, S. J. Niu, S. Krueger, and T. Wagner, 2013b: Exploring parameterization for turbulent entrainment-mixing processes in clouds. *J. Geophys. Res.*, **118,** 185-194, doi: 10.1029/2012jd018464.

Luke, E. P., and P. Kollias, 2013: Separating Cloud and Drizzle Radar Moments during Precipitation Onset Using Doppler Spectra. *J. Atmos. Oceanic Technol.*, **30,** 1656-1671, doi: 10.1175/jtech-d-11-00195.1.

Mann, J. A. L., J. C. Chiu, R. J. Hogan, E. J. O'Connor, T. S. L'Ecuyer, T. H. M. Stein, and A. Jefferson, 2014: Aerosol impacts on drizzle properties in warm clouds from ARM Mobile Facility maritime and continental deployments. *J. Geophys. Res.*, **119,** 4136-4148, doi: 10.1002/2013jd021339.

Mather, J. H., and J. W. Voyles, 2013: THE ARM CLIMATE RESEARCH FACILITY A Review of Structure and Capabilities. *Bull. Am. Meteorol. Soc.*, **94,** 377-392, doi: 10.1175/bams-d-11-00218.1.

Accepted for publication in *Bulletin of the American Meteorological Society*. DOI 10.1175/BAMS-D-19-0220.1.

Mayer, K. J., and Coauthors, 2020: Secondary Marine Aerosol Plays a Dominant Role over Primary Sea Spray Aerosol in Cloud Formation. *ACS Central Science*, **6,** 2259-2266, doi: 10.1021/acscentsci.0c00793.

Mechem, D. B., S. E. Yuter, and S. P. de Szoeke, 2012: Thermodynamic and Aerosol Controls in Southeast Pacific Stratocumulus. *J. Atmos. Sci.*, **69,** 1250-1266, doi: 10.1175/jas-d-11-0165.1.

Mechem, D. B., C. S. Wittman, M. A. Miller, S. E. Yuter, and S. P. De Szoeke, 2018: Joint Synoptic and Cloud Variability over the Northeast Atlantic near the Azores. *J. Appl. Meteorol. Clim.*, **57,** 1273-1290, doi: 10.1175/jamc-d-17-0211.1.

Mei, F., A. Setyan, Q. Zhang, and J. Wang, 2013a: CCN activity of organic aerosols observed downwind of urban emissions during CARES. *Atmos. Chem. Phys.*, **13,** 12155-12169.

Mei, F., and Coauthors, 2013b: Droplet activation properties of organic aerosols observed at an urban site during CalNex-LA. *J. Geophys. Res.*, **118,** 2903-2917 doi: 10.1002/jgrd.50285.

Mungall, E. L., and Coauthors, 2017: Microlayer source of oxygenated volatile organic compounds in the summertime marine Arctic boundary layer. *Proc. Natl. Acad. Sci.*, **114,** 6203-6208, doi: 10.1073/pnas.1620571114.

Nguyen, C., and V. Chandrasekar, 2014: An Improved Method for Detecting and Separating Cloud from Drizzle Radar Signatures Using a Time Domain Parametric Technique. *AGU Fall Meeting*, San Francisco, California.

Nicholls, S., and J. Leighton, 1986: An observation study of the structure of stratiform cloud sheets: Part I. Structure. *Q. J. Roy. Meteor. Soc.*, **112,** 431-460, doi: 10.1002/qj.49711247209.

O'Dowd, C. D., and Coauthors, 2004: Biogenically driven organic contribution to marine aerosol. *Nature*, **431,** 676-680.

O'Connor, E. J., R. J. Hogan, and A. J. Illingworth, 2005: Retrieving stratocumulus drizzle parameters using Doppler radar and lidar. *Journal of Applied Meteorology*, **44,** 14-27.

Ovadnevaite, J., and Coauthors, 2014: Submicron NE Atlantic marine aerosol chemical composition and abundance: Seasonal trends and air mass categorization. *J. Geophys. Res.*, **119,** 11850-11863, doi: 10.1002/2013jd021330.

Painemal, D., and P. Zuidema, 2013: The first aerosol indirect effect quantified through airborne remote sensing during VOCALS-REx. *Atmos. Chem. Phys.*, **13,** 917-931, doi: 10.5194/acp-13-917-2013.

Petters, M. D., and S. M. Kreidenweis, 2007: A single parameter representation of hygroscopic growth and cloud condensation nucleus activity. *Atmos. Chem. Phys.*, **7,** 1961-1971, doi: 10.5194/acp-7-1961-2007.

Petters, M. D., J. R. Snider, B. Stevens, G. Vali, I. Faloona, and L. M. Russell, 2006: Accumulation mode aerosol, pockets of open cells, and particle nucleation in the remote subtropical Pacific marine boundary layer. *J. Geophys. Res.*, **111**, doi: 10.1029/2004jd005694.

Pinsky, M., and A. Khain, 2018: Theoretical Analysis of the Entrainment-Mixing Process at Cloud Boundaries. Part I: Droplet Size Distributions and Humidity within the Interface Zone. *J. Atmos. Sci.*, **75,** 2049-2064, doi: 10.1175/jas-d-17-0308.1.

Accepted for publication in *Bulletin of the American Meteorological Society*. DOI 10.1175/BAMS-D-19-0220.1.

Prather, K. A., and Coauthors, 2013: Bringing the ocean into the laboratory to probe the chemical complexity of sea spray aerosol. *Proc. Natl. Acad. Sci.*, **110,** 7550-7555, doi: 10.1073/pnas.1300262110.

Quinn, P. K., and T. S. Bates, 2011: The case against climate regulation via oceanic phytoplankton sulphur emissions. *Nature*, **480,** 51-56, doi: 10.1038/nature10580.

Quinn, P. K., D. B. Collins, V. H. Grassian, K. A. Prather, and T. S. Bates, 2015: Chemistry and Related Properties of Freshly Emitted Sea Spray Aerosol. *Chemical Reviews*, **115,** 4383-4399, doi: 10.1021/cr500713g.

Raes, F., 1995: Entrainment of free tropospheric aerosols as regulating mechanism form cloud condensation nuclei in the remote marine boundary layer. *J. Geophys. Res.*, **100,** 2893-2903, doi: 10.1029/94jd02832.

Remillard, J., and G. Tselioudis, 2015: Cloud Regime Variability over the Azores and Its Application to Climate Model Evaluation. *J. Climate*, **28,** 9707-9720, doi: 10.1175/jcli-d-15-0066.1.

Rosenfeld, D., S. Sherwood, R. Wood, and L. Donner, 2014a: Climate Effects of Aerosol-Cloud Interactions. *Science*, **343,** 379-380.

Rosenfeld, D., and Coauthors, 2014b: Global observations of aerosol-cloud-precipitation-climate interactions. *Rev. Geophys.*, **52,** 750-808, doi: 10.1002/2013RG000441.

Rusli, S. P., D. P. Donovan, and H. W. J. Russchenberg, 2017: Simultaneous and synergistic profiling of cloud and drizzle properties using ground-based observations. *Atmos. Meas. Tech.*, **10,** 4777-4803, doi: 10.5194/amt-10-4777-2017.

Russell, L. M., and Coauthors, 1998: Bidirectional mixing in an ACE 1 marine boundary layer overlain by a second turbulent layer. *J. Geophys. Res.*, **103,** 16411-16432, doi: 10.1029/97jd03437.

Schmid, B., and Coauthors, 2014: The DOE ARM aerial facility. *Bull. Am. Meteorol. Soc.*, **95,** 723-742, doi: 10.1175/bams-d-13-00040.1.

Siebert, H., and Coauthors, 2020: Observations of aerosol, cloud, turbulence, and radiation properties at the top of the marine boundary layer over the Eastern North Atlantic Ocean: The ACORES campaign. *Bull. Am. Meteorol. Soc.***,** 1-59, doi: 10.1175/bams-d-19-0191.1.

Sorooshian, A., G. Feingold, M. D. Lebsock, H. L. Jiang, and G. L. Stephens, 2010: Deconstructing the precipitation susceptibility construct: Improving methodology for aerosol-cloud precipitation studies. *J. Geophys. Res.*, **115**, doi: 10.1029/2009jd013426.

Stephens, G. L., and Coauthors, 2010: Dreary state of precipitation in global models. *J. Geophys. Res.*, **115**, doi: 10.1029/2010jd014532.

Stevens, B., and G. Feingold, 2009: Untangling aerosol effects on clouds and precipitation in a buffered system. *Nature*, **461,** 607-613, doi: 10.1038/nature08281.

Terai, C. R., R. wood, and T. L. Kubar, 2015: Satellite and diagnostic model estimates of precipitation susceptibility in low-level, marine stratocumulus. *Submitted to journal of Geophysical Research*.

Terai, C. R., R. Wood, D. C. Leon, and P. Zuidema, 2012: Does precipitation susceptibility vary with increasing cloud thickness in marine stratocumulus? *Atmos. Chem. Phys.*, **12,** 4567-4583, doi: 10.5194/acp-12-4567-2012.

Accepted for publication in *Bulletin of the American Meteorological Society*. DOI 10.1175/BAMS-D-19-0220.1.

Thalman, R., and Coauthors, 2017: CCN activity and organic hygroscopicity of aerosols downwind of an urban region in central Amazonia: seasonal and diel variations and impact of anthropogenic emissions. *Atmos. Chem. Phys.*, **17,** 11779-11801, doi: 10.5194/acp-17-11779-2017.

Twomey, S., 1977: Influence of pollution on shortwave albedo of clouds. *J. Atmos. Sci.*, **34,** 1149-1152.

Wang, J., X. Dong, and R. Wood, 2016a: Aerosol and Cloud Experiments in Eastern North Atlantic (ACE-ENA) Science Plan.

Wang, J., M. Pikridas, S. R. Spielman, and T. Pinterich, 2017: A fast integrated mobility spectrometer for rapid measurement of sub-micrometer aerosol size distribution, Part I: Design and model evaluation. *J. Aerosol Sci.*, **108,** 44-55, doi: 10.1016/j.jaerosci.2017.02.012.

Wang, J., and Coauthors, 2009: Observations of marine stratocumulus microphysics and implications for processes controlling droplet spectra: Results from the Marine Stratus/Stratocumulus Experiment. *J. Geophys. Res.*, **114**, doi: 10.1029/2008jd011035.

Wang, J., and Coauthors, 2019a: Cloud droplet activation of secondary organic aerosol is mainly controlled by molecular weight, not water solubility. *Atmos. Chem. Phys.*, **19,** 941-954, doi: 10.5194/acp-19-941-2019.

Wang, J., and Coauthors, 2019b: Aerosol and Cloud Experiments in Eastern North

Atlantic (ACE-ENA) Field Campaign Report.

Wang, J., and Coauthors, 2016b: Amazon boundary layer aerosol concentration sustained by vertical transport during rainfall. *Nature*, **539,** 416-419, doi: 10.1038/nature19819.

Wang, Q., and B. A. Albrecht, 1994: Observations of cloud-top entrainment in marine stratocumulus clouds. *J. Atmos. Sci.*, **51,** 1530-1547, doi: 10.1175/1520-0469(1994)051<1530:ooctei>2.0.co;2.

Wang, Y., T. Pinterich, and J. Wang, 2018: Rapid measurement of sub-micrometer aerosol size distribution using a fast integrated mobility spectrometer. *J. Aerosol Sci.*, **121,** 12-20, doi: 10.1016/j.jaerosci.2018.03.006.

Wang, Y., and Coauthors, 2021: Vertical profiles of trace gas and aerosol properties over the Eastern North Atlantic: Variations with season and synoptic condition. *Atmos. Chem. Phys. Discuss.*

Warner, J., 1973: Microstructure of cumulus cloud .4. Effect on droplet spectrum of mixing between cloud and environment. *J. Atmos. Sci.*, **30,** 256-261.

Westbrook, C. D., R. J. Hogan, E. J. O'Connor, and A. J. Illingworth, 2010: Estimating drizzle drop size and precipitation rate using two-colour lidar measurements. *Atmos. Meas. Tech.*, **3,** 671-681, doi: 10.5194/amt-3-671-2010.

Willis, M. D., and Coauthors, 2017: Evidence for marine biogenic influence on summertime Arctic aerosol. *Geophys. Res. Lett.*, **44,** 6460-6470, doi: 10.1002/2017gl073359.

Wood, R., 2007: Cancellation of aerosol indirect effects in marine stratocumulus through cloud thinning. *J. Atmos. Sci.*, **64,** 2657-2669, doi: 10.1175/jas3942.1.

——, 2012: Stratocumulus Clouds. *Mon. Weather Rev.*, **140,** 2373-2423, doi: 10.1175/mwr-d-11-00121.1.

Accepted for publication in *Bulletin of the American Meteorological Society*. DOI 10.1175/BAMS-D-19-0220.1.

Wood, R., T. L. Kubar, and D. L. Hartmann, 2009: Understanding the importance of microphysics and macrophysics for warm rain in marine low clouds: Part II. Heuristic models of rain formation. *J. Atmos. Sci.*, **66,** 2973-2990, doi: doi: 10.1175/2009JAS3072.1.

Wood, R., D. Leon, M. Lebsock, J. Snider, and A. D. Clarke, 2012: Precipitation driving of droplet concentration variability in marine low clouds. *J. Geophys. Res.*, **117**, doi: 10.1029/2012jd018305.

Wood, R., C. S. Bretherton, D. Leon, A. D. Clarke, P. Zuidema, G. Allen, and H. Coe, 2011: An aircraft case study of the spatial transition from closed to open mesoscale cellular convection over the Southeast Pacific. *Atmos. Chem. Phys.*, **11,** 2341-2370, doi: 10.5194/acp-11-2341-2011.

Wood, R., and Coauthors, 2015: Clouds, Aerosol, and Precipitation in the Marine Boundary Layer: An ARM Mobile Facility Deployment. *Bull. Am. Meteorol. Soc.*, **96,** 419-439, doi: 10.1175/BAMS-D-13-00180.1.

Wu, P., X. Q. Dong, and B. K. Xi, 2015: Marine boundary layer drizzle properties and their impact on cloud microphysical property retrievals. *Atmos. Meas. Tech.*, **8,** 3555-3562, doi: 10.5194/amt-8-3555-2015.

Wu, P., X. Q. Dong, B. K. Xi, J. J. Tian, and D. M. Ward, 2020: Profiles of MBL Cloud and Drizzle Microphysical Properties Retrieved From Ground-Based Observations and Validated by Aircraft In Situ Measurements Over the Azores. *J. Geophys. Res.*, **125**, doi: 10.1029/2019jd032205.

Wyant, M., R. Wood, and S. Pennypacker, 2020: Seasonal contrasts in aerosol-cloud-precipitation interactions in marine low clouds during ACE-ENA. *Manuscript in preparation*.

Wyant, M. C., and Coauthors, 2015: Global and regional modeling of clouds and aerosols in the marine boundary layer during VOCALS: the VOCA intercomparison. *Atmos. Chem. Phys.*, **15,** 153-172, doi: 10.5194/acp-15-153-2015.

Yeom, J. M., S. S. Yum, Y. A. Liu, and C. S. Lu, 2017: A study on the entrainment and mixing process in the continental stratocumulus clouds measured during the RACORO campaign. *Atmos. Res.*, **194,** 89-99, doi: 10.1016/j.atmosres.2017.04.028.

Yeom, J. M., and Coauthors, 2020: Vertical variation of cloud microphysics and its implication for the entrainment-mixing process in marine stratocumulus clouds measured during the ACE-ENA campaign. *J. Geophys. Res.*, **In review**.

Yum, S. S., J. Wang, Y. G. Liu, G. I. Senum, S. R. Springston, R. L. McGraw, and J. M. Yeom, 2015: Cloud microphysical relationships and their implication on entrainment and mixing mechanism for the stratocumulus clouds measured during the VOCALS project. *J. Geophys. Res.*, **120,** 5047-5069, doi: 10.1002/2014JD022802.

Zawadowicz, M. A., and Coauthors, 2021: Aircraft measurements of aerosol and trace gas chemistry in the Eastern North Atlantic. *Atmos. Chem. Phys.*, **In press**, doi: 10.5194/acp-2020-887.

Zhang, Z., and Coauthors, 2020: Vertical Dependence of Horizontal Variation of Cloud Microphysics: Observations from the ACE-ENA field campaign and implications for warm rain simulation in climate models. *Atmos. Chem. Phys. Discuss.*, **2020,** 1-46, doi: 10.5194/acp-2020-788.

Accepted for publication in *Bulletin of the American Meteorological Society*. DOI 10.1175/BAMS-D-19-0220.1.

Zheng, G., C. Kuang, J. Uin, T. Watson, and J. Wang, 2020a: Large contribution of organics to condensational growth and formation of cloud condensation nuclei (CCN) in remote marine boundary layer. *Atmos. Chem. Phys.*, **20,** 12515-12525, doi: 10.5194/acp-20-12515-2020.

Zheng, G., and Coauthors, 2020b: New particle formation in the remote marine boundary layer. *Nature Communications*, **In press**, doi: 10.1038/s41467-020-20773-1.

Zheng, G. J., and Coauthors, 2020c: Long-range transported North American wildfire aerosols observed in marine boundary layer of eastern North Atlantic. *Environment International*, **139**, doi: 10.1016/j.envint.2020.105680.

Zheng, G. J., and Coauthors, 2018: Marine boundary layer aerosol in the eastern North Atlantic: seasonal variations and key controlling processes. *Atmos. Chem. Phys.*, **18,** 17615-17635, doi: 10.5194/acp-18-17615-2018.

Accepted for publication in *Bulletin of the American Meteorological Society.* DOI 10.1175/BAMS-D-19-0220.1.

FIGURES

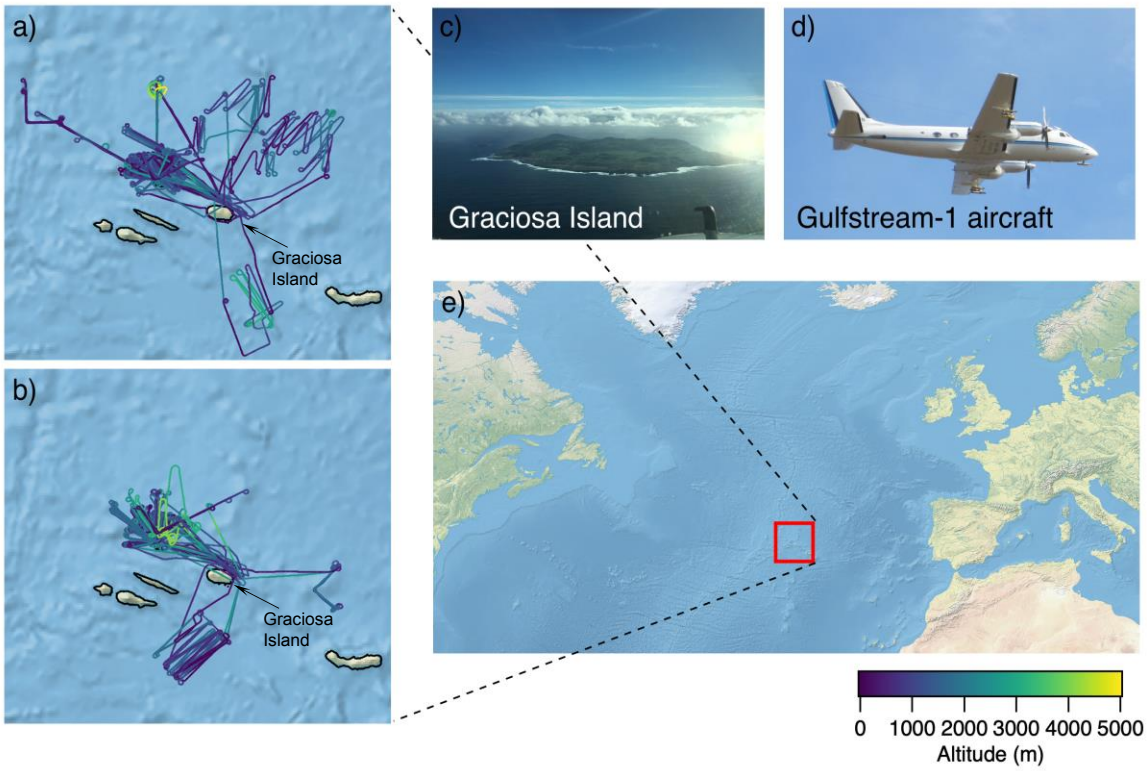

Figure 1. The fight paths of the G-1 research aircraft colored by altitude during (a) the summer IOP and (b) the winter IOP. Most of the flight paths are in the vicinity of the ENA site on Graciosa Island (c). A photo of the G-1 aircraft is shown in (d), and the general geographic location of the sampling area is shown in (e).

Accepted for publication in *Bulletin of the American Meteorological Society*. DOI 10.1175/BAMS-D-19-0220.1.

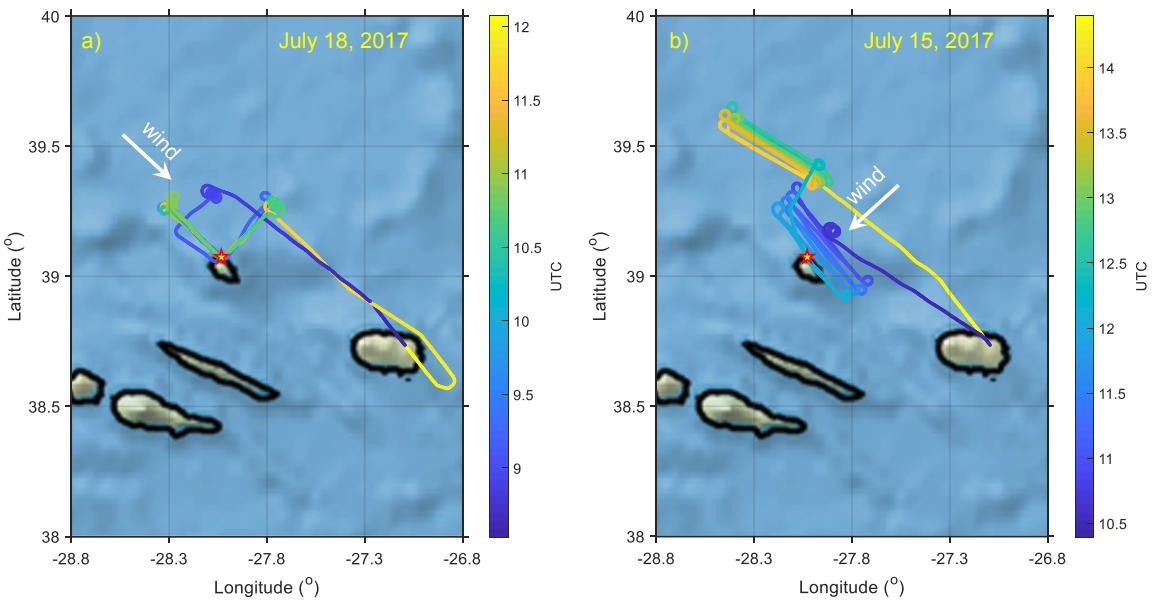

Figure 2. Examples of G-1 flight paths during the ACE-ENA colored by UTC time. (a) L-shape patterns consisting of ~ 30 km upwind and crosswind legs at different altitudes on July 18, 2017, with the "corner" of L-pattern above the ENA site, (b) Lagrangian drift pattern consisting of crosswind stacks of several straight and level runs approximately 60 km in length below, in, and above cloud on July 15, 2017. The white arrow indicates the wind direction, and the star represents the location of the ENA site on Graciosa Island.

Accepted for publication in *Bulletin of the American Meteorological Society*. DOI 10.1175/BAMS-D-19-0220.1.

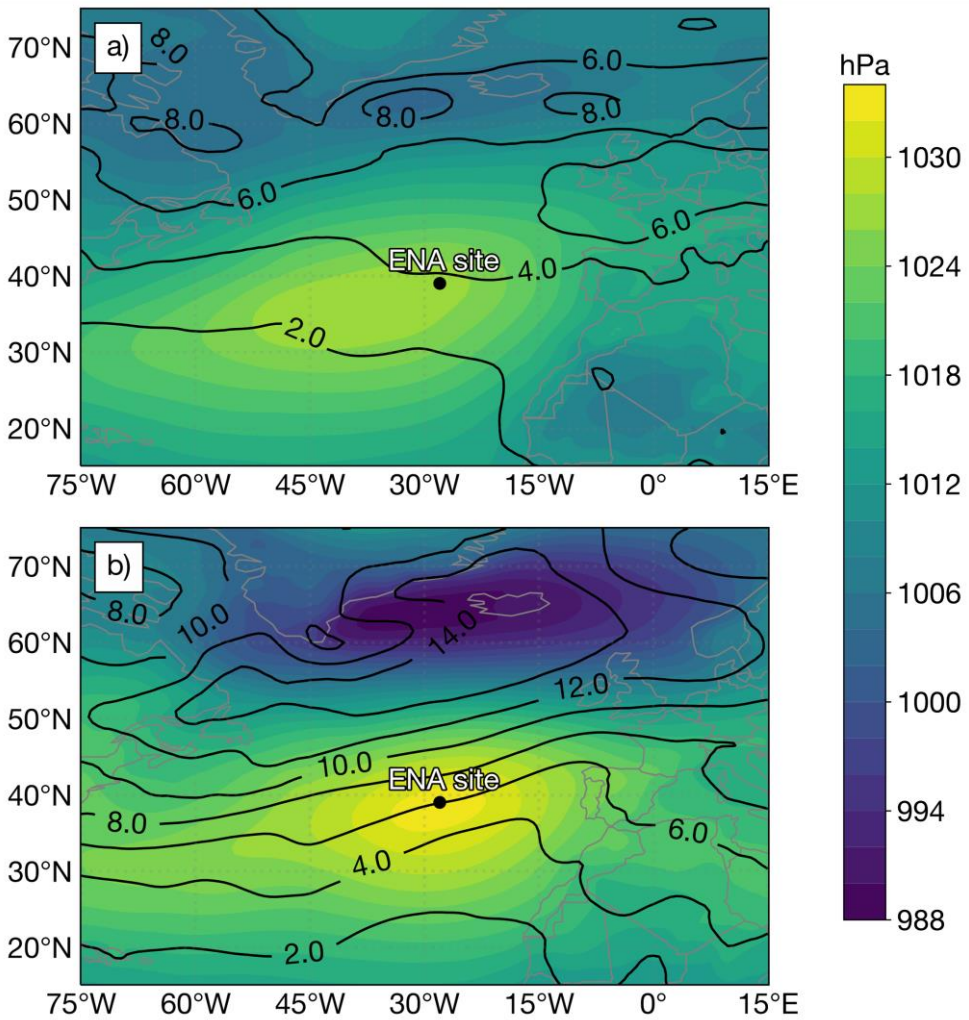

Figure 3. The average mean sea level pressure (MSLP; color-filled contours) and standard deviation of MSLP (black-contours) across the (a) summer and (b) winter IOPs generated using the six-hourly ECMWF interim reanalysis (ERA-Interim; Dee et al. 2011).

Accepted for publication in *Bulletin of the American Meteorological Society*. DOI 10.1175/BAMS-D-19-0220.1.

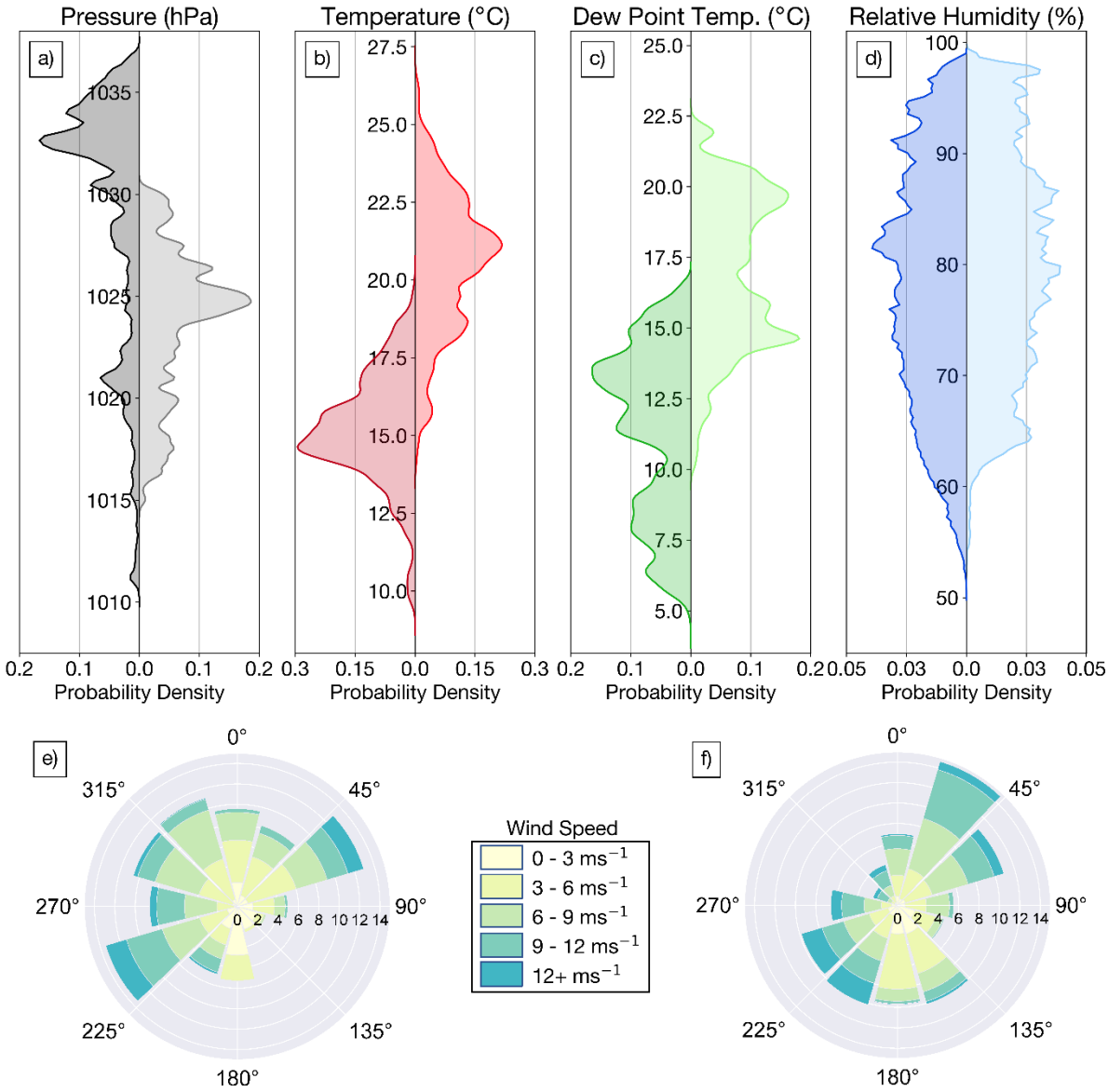

Figure 4. Kernel density estimation of (a) sea level pressure, (b) temperature at 2 m, (c) dew point and 2 m, and (d) relative humidity at 2 m measured at the ENA atmospheric observatory on Graciosa Island. The left (right) side of the plots represents the probability density during the winter (summer) IOP. Wind rose plots represent the surface wind conditions observed across the (e) summer and (f) winter IOPs.

Accepted for publication in *Bulletin of the American Meteorological Society*. DOI 10.1175/BAMS-D-19-0220.1.

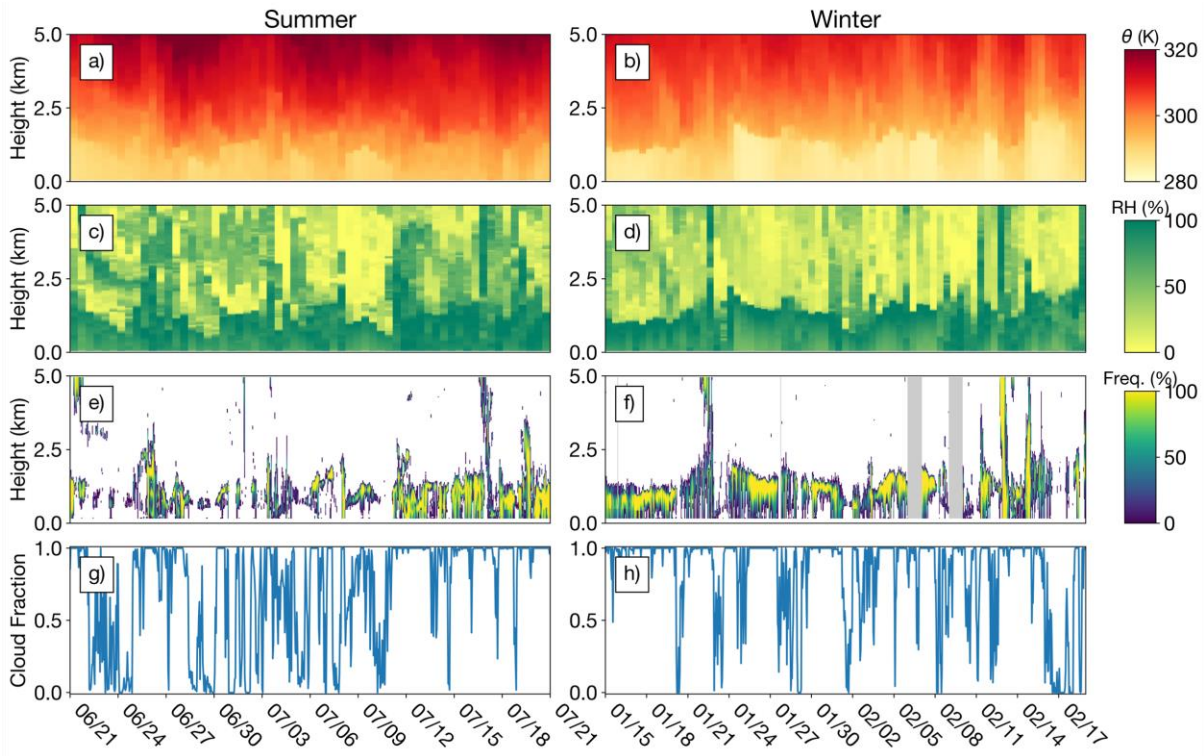

Figure 5. The (a, b) potential temperature and (c, d) relative humidity profiles measured by alternating 11:30 and 23:30 UTC (11:30 and 23:30 local in the summer and 12:30 and 00:30 local in the winter) radiosonde launches from Graciosa Island. The (e, f) radar-derived hydrometeor frequency of occurrence (Kollias et al. 2007) and (g, h) lidar-derived total cloud fraction below 4 km. The left and right columns represent conditions during the summer and winter IOPs, respectively. Gray areas in (f) denote times when the cloud radar was unavailable and thus no hydrometeor retrievals are made.

Accepted for publication in *Bulletin of the American Meteorological Society*. DOI 10.1175/BAMS-D-19-0220.1.

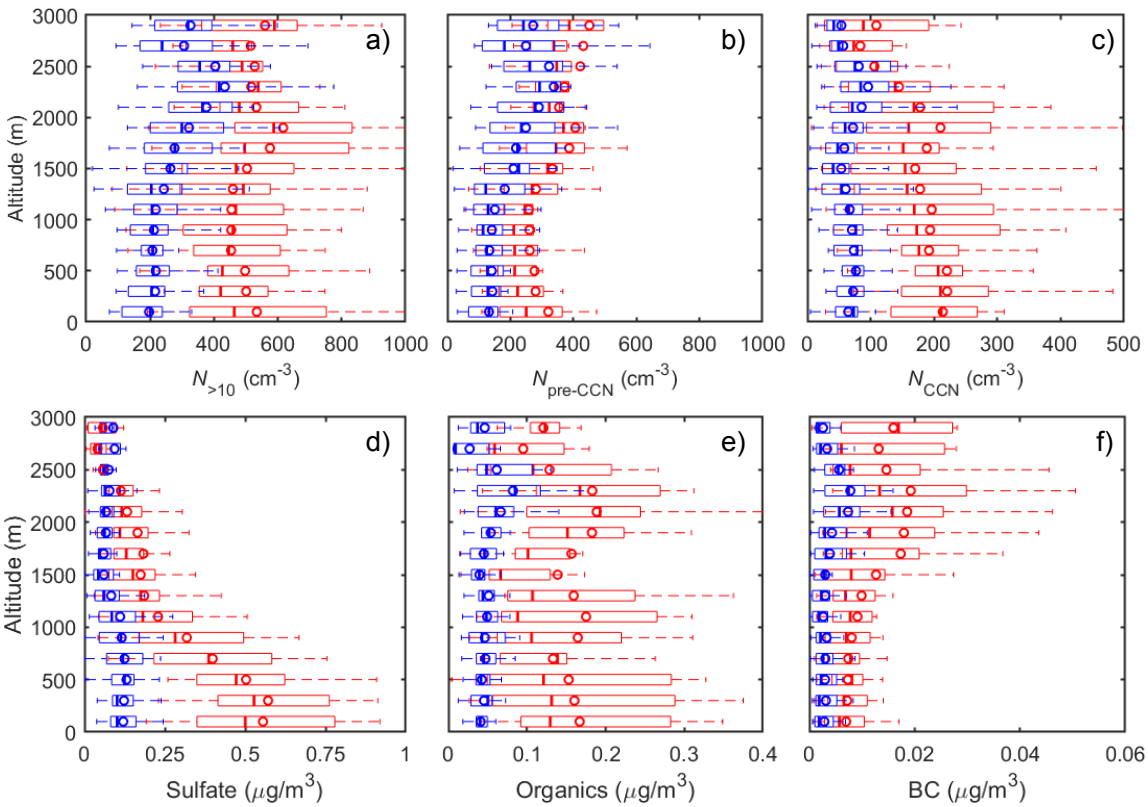

Figure 6. Vertical profiles of (a) the concentrations of particles larger than 10 nm ($N_{>10}$), (b) concentrations of pre-CCN particles (i.e., particles that are too small to form cloud droplet under average conditions inside MBL, $N_{\text{pre-CCN}}$), (c) the concentrations of cloud condensation nuclei, (d) mass concentrations of sulfate, (e) mass concentrations of organics, and (f) mass concentrations of black carbon (BC) in the ENA during the summer (red) and winter (blue) IOPs. $N_{\text{pre-CCN}}$ is derived as the difference between $N_{>10}$ and the CCN concentration, which is calculated by integrating the bimodal size distribution measured by the FIMS for particles with diameter larger than the Hoppel minimum. The box whisker plots show 10th, 25th, 50th, 75th, and 90th percentiles, respectively, and the circle markers represent the mean values.

Accepted for publication in *Bulletin of the American Meteorological Society*. DOI 10.1175/BAMS-D-19-0220.1.

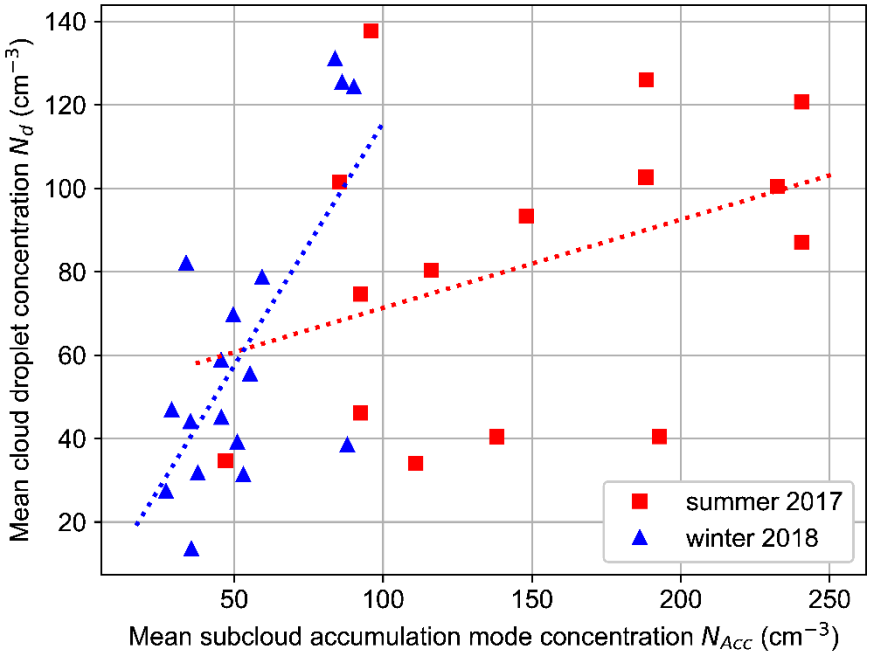

Figure 7. Flight mean cloud droplet concentration (N_d) from all in-cloud samples plotted against the mean BL accumulation mode (i.e., particles with diameter above 100 nm) concentration N_{Acc} measured by a Passive Cavity Aerosol Spectrometer (PCASP), for summer (red) and winter (blue) flights.

Accepted for publication in *Bulletin of the American Meteorological Society*. DOI 10.1175/BAMS-D-19-0220.1.

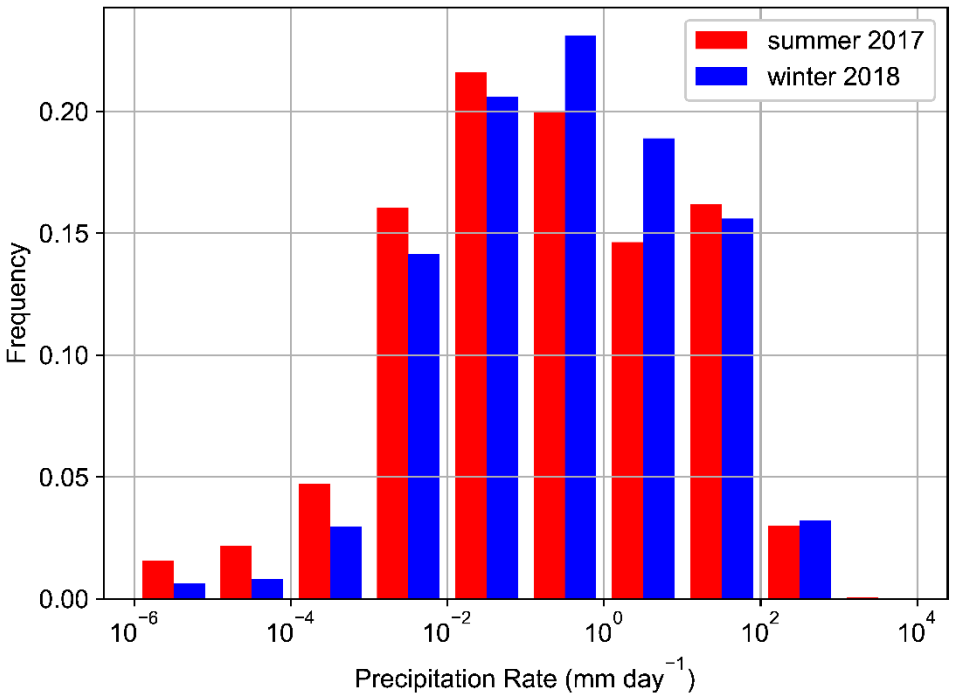

Figure 8. Histogram of in-cloud precipitation rate estimated from the 2D-S probe measurements onboard the G-1 during the summer (red) and winter (blue) IOPs. Although there is little seasonal contrast in the highest rates, there is a shift toward higher intermediate rates (0.1-10 mm day^{-1}) during winter.

Accepted for publication in *Bulletin of the American Meteorological Society*. DOI 10.1175/BAMS-D-19-0220.1.

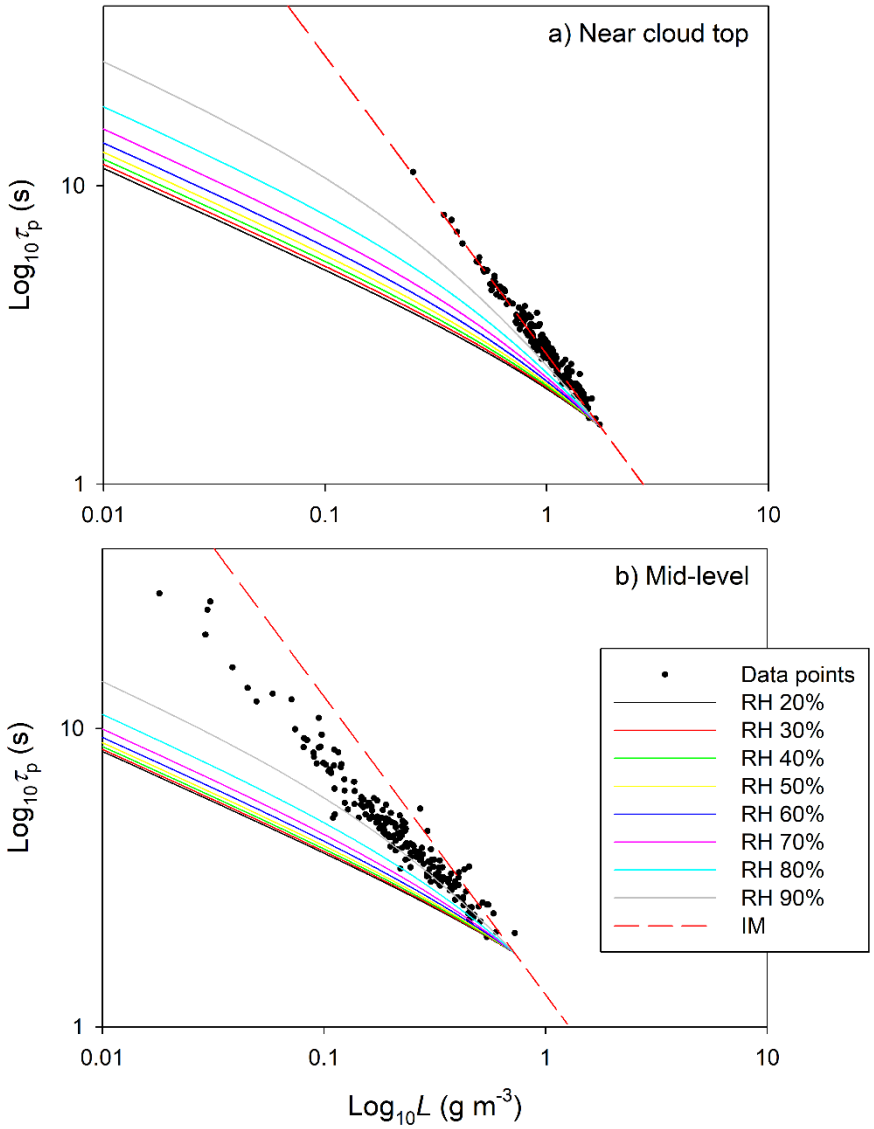

Figure 9. Examples of $\mathrm{Log}_{10}L$-$\mathrm{Log}_{10}\tau_p$ mixing diagram for near cloud top (a) and mid-level (b) horizontal penetrations during the flight on July 18, 2017. The dashed line indicates the expected data trend for extreme inhomogeneous mixing (IM) and the solid lines indicate the expected trends for homogeneous mixing with different RH of entraining air. The phase relaxation time (τ_p) and liquid water content (L) are derived from droplet size spectrum measured by the FCDP.

Accepted for publication in *Bulletin of the American Meteorological Society*. DOI 10.1175/BAMS-D-19-0220.1.

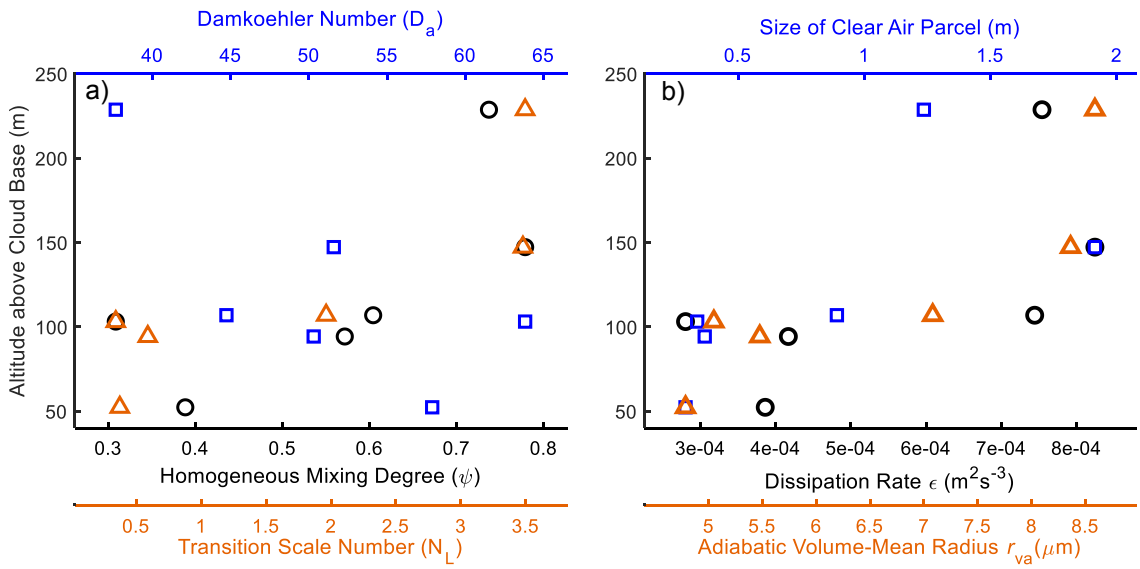

Figure 10. An example of height dependence of turbulent entrainment-mixing processes and related quantities (Flight on 6/28/2017, Summer IOP RF05), where ψ, D_a, N_L, ε, and r_{va} denote the homogeneous mixing degree, Damkoehler number, transition scale number, turbulent dissipation rate, and adiabatic mean volume radius, respectively. The cloud droplet size distributions were measured with a Fast Cloud Droplet Probe (FCDP) at 10 Hz. Humidity was measured with an Open Path Tunable Diode Laser Hygrometer (Diskin et al., 2002) at 10 Hz. Air temperature, air pressure, and altitude were measured with the Aircraft Integrated Meteorological Measurement System (AIMMS) at 20 Hz. Turbulent dissipation rate is derived from the 20 Hz AIMMS-20 air motion measurements.

Accepted for publication in *Bulletin of the American Meteorological Society*. DOI 10.1175/BAMS-D-19-0220.1.

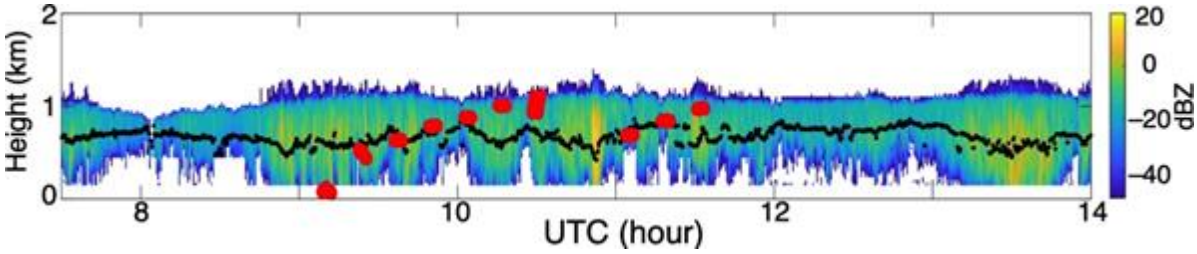

Figure 11. Time-height radar reflectivity profiles on 18 July 2017 during the ACE–ENA campaign. The black dots represent cloud base heights, determined using a threshold in attenuated lidar backscatter of 0.00005 m^{-1} sr^{-1}. The big red dots indicate the G-1 aircraft flight height and time.

Accepted for publication in *Bulletin of the American Meteorological Society.* DOI 10.1175/BAMS-D-19-0220.1.

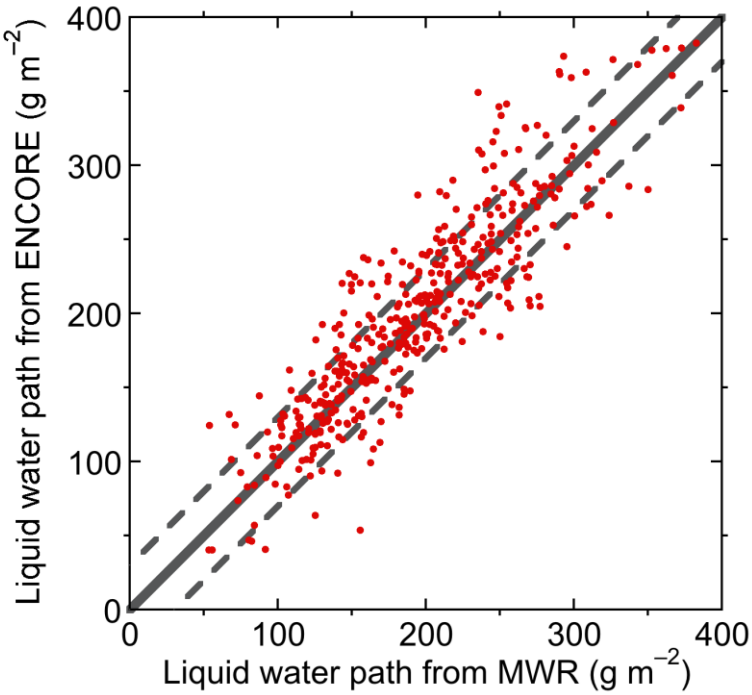

Figure 12. A scatter plot of retrieved liquid water paths from ENCORE vs. those from microwave radiometer observations. The solid line represents the 1:1 line, while the dash lines depart ± 30 g m^{-2} from the solid line.

Accepted for publication in *Bulletin of the American Meteorological Society*. DOI 10.1175/BAMS-D-19-0220.1.

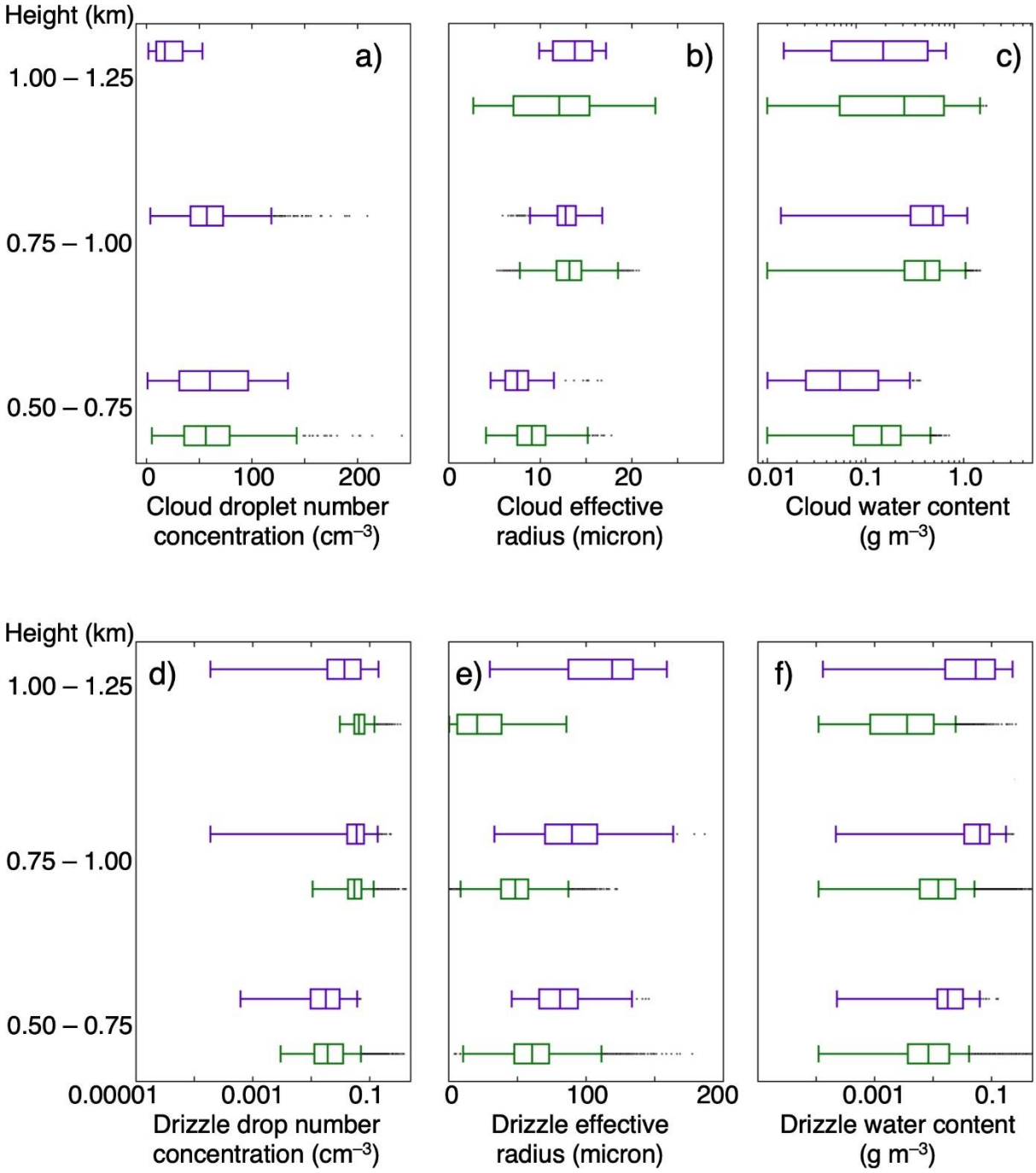

Figure 13. Box plots of (a) cloud droplet number concentration, (b) cloud effective radius and (c) cloud water content calculated from in-situ measurements (blue) and from ENCORE retrievals (red) on 18 July 2017. The boundaries of each box represent the 25% and 75% quartiles, and the line inside the box represents the median. The whiskers mark the range within

Accepted for publication in *Bulletin of the American Meteorological Society*. DOI 10.1175/BAMS-D-19-0220.1.

1.5 times the interquartile distance. Note that the retrieved cloud droplet number concentration in (a) is independent of height, and thus is only plotted once and placed in the altitude bin of 0.5–0.75 km. (d)–(f) are same as (a)–(c), but for drizzle properties. In-situ size distributions were used only when the aircraft was within 10 km of the ENA site. The final sample size is about 1800 profiles.

Accepted for publication in *Bulletin of the American Meteorological Society.* DOI 10.1175/BAMS-D-19-0220.1.